Amplified-Spontaneous-Emission Feedback Circuit Technique with Improved Optical Power Resolutions

BISWAS BISWAJIT
Photonics Laboratory

Supervisor:

Prof. Dr. Hiroji Masuda

Assistant supervisor:

Prof. Dr. Yasuhisa Fujita

Prof. Dr. Hiroyuki Kageshima

Prof. Dr. Wenchang Yeh

Graduate School of Natural Science and Technology
Shimane University, Japan
September 2023

Acknowledgment

I want to sincerely thank everyone who helped support and contribute to completing this thesis.

I would like to start by expressing my gratitude to my honorable supervisor, Professor Dr. Hiroji Masuda, for his advice, knowledge, and ongoing support throughout the entire research process. His invaluable insights, constructive feedback, and unwavering encouragement have been instrumental in shaping this thesis and enhancing its quality. I am also grateful to the Assistant Professor Dr. Kokoro Kitamura for his support and encouragement.

My sincere gratitude goes out to the co-authors of this study for being so willing to share their time, wisdom, and experiences with us. Their contribution has been vital in collecting the necessary data and achieving the objectives of this research.

I would like to thank the JSPS KAKENHI Grant-in-Aid for Scientific Research 19K004410, 22K04140, and JST (Japan Science and Technology) for their financial assistance. Without their financial assistance, this research would not have been possible.

I am indebted to my friends and colleagues who have provided their support and encouragement throughout this journey. Their words of encouragement and moral support have been invaluable in overcoming challenges and maintaining my enthusiasm.

Lastly, I want to thank my family from the bottom of my heart. The foundation of my academic endeavors has been their unwavering love, tolerance, and understanding. Their constant belief in my abilities has given me the strength to overcome obstacles and reach this milestone.

In conclusion, I am truly grateful to Professor Dr. Hiroji Masuda, Professor Dr. Yasuhisa Fujita, and all my co-supervisors who have contributed to this thesis in various ways. Your support, guidance, and encouragement have played a significant role in shaping this work, and I am sincerely thankful for your contributions.

Biswas Biswajit

List of Figures

1. Introduction

No figure

2. Fundamentals

3. ASEFC scheme for Optical Power Sensing

4. Temperature-controlled ASEFC with improved OPR for Optical Power Sensing

5. Bandwidth and Dynamic range Characteristics of ASEFC

List of Publications

Journal Articles

1. Hiroji Masuda, **Biswajit Biswas**, Md Syful Islam and Kokoro Kitamura, “Amplified-spontaneous emission feedback circuit scheme for optical measurement with improved optical power resolutions,” IEICE Communications Express, Vol.1, 1–6, [Accepted: October 25, 2021]. https://doi.org/10.1587/comex.2021XBL0189
2. **Biswajit Biswas**, MD Golam Barkatul Abrar, Kunihiro Tanaka, Ryuga Harada, Kokoro Kitamura, and Hiroji Masuda, “High-resolution and Stable optical power measurement using a temperature controlled amplified-spontaneous-emission feedback circuit, IEICE Communications Express,” Vol.1, 1–6, [Accepted: February 20, 2023]. https://doi.org/10.1587/comex.2023XBL0014
3. **Biswajit Biswas**, MD Golam Barkatul Abrar, Kunihiro Tanaka, Ryuga Harada, Kokoro Kitamura, and Hiroji Masuda, “Amplified-spontaneous-emission feedback circuit with wide operating bandwidth and dynamic range,” IEICE Electronics Express. [Accepted: July 11, 2023]. https://doi.org/10.1587/elex.20.20230229

Conference Papers

As the first author.

1. **B. Biswas**, MD S. Islam, K. Kitamura, and H. Masuda, “Output Wavelength Dependence of the Performance of an Optically Amplified Feedback Circuit,” IEICE Society Conference, B-13-2 (2019).
2. **B. Biswas**, MD S. Islam, K. Kitamura, and H. Masuda, “Optimization of the Output Wavelength of an Optically Amplified Feedback Circuit for a Multi-wavelength Optical Sensing System,” HISS, 21st, B1-22, pp.332-334(2019), (Domestic Conference with Review).
3. **B. Biswas**, H. Masuda, MD S. Islam, and K. Kitamura, “Numerical Simulation on Wavelength Characteristics of an Optically Amplified Feedback Circuit for Multi-Wavelength Sensing Applications,”The67thJSAPSpringMeeting, 14p-B409-15(2020).
4. **B. Biswas** and H. Masuda, “Numerical Simulation on the Performance of an Amplified-Spontaneous- Emission Feedback Circuit in Optical Power Sensing Application,” IEICE General Conference, B-13-10 (2021).
5. **B. Biswas** and H. Masuda, “Remote Temperature Sensing with an Amplified-Spontaneous-Emission Feedback Circuit,” IEICE Society Conference, B-13-2 (2021).
6. **B. Biswas**, H. Masuda and Kunihiro Tanaka, “Fiber-Optic Multipoint Temperature Sensing Scheme Using Amplified Spontaneous Emission of Erbium-Doped Fiber,” The 72nd Annual Meeting of the Chugoku Branch of the Electrical and Information Society (2021).

As the Co-author.

1. H. Masuda, K. Kitamura, MD S. Islam, **B. Biswas**, and T. Kanou, “Optically-amplified feedback photo-detector with significantly small resolution,” 11a-W935-7 (in Japanese), The 66th JSAP Spring Meeting (2019).
2. Hiroji Masuda, Kokoro Kitamura, MD Syful Islam, and **Biswajit Biswas**, “Optically-amplified feedback circuit with high improvements in optical power resolution,” MC2-5, The 24th

Optoelectronics and Communications Conference (OECC) (2019) (International Conference with Review). https://DOI:10.23919/PS.2019.8817895

3. MD Syful Islam, **Biswas Biswajit**, K. Kitamura and H. Masuda, "Loop Loss Dependence of the Performance of an Optically Amplified Feedback Circuit," B-13-3, IEICE Society Conference (2019).
4. MD Syful Islam, **Biswas Biswajit**, K. Kitamura and H. Masuda, "Optimization of the Loop Loss of an Optically Amplified Feedback Circuit for Optical Power Sensing Systems," A1-22, pp. 69-71, HISS 21st Conference (2019) (Domestic Conference with Review).
5. Md Syful Islam, Hiroji Masuda, **Biswajit Biswas**, and Kokoro Kitamura, "Numerical Simulation on the Loop-loss Dependence of the Performance of an Optically Amplified Feedback Circuit," 14p-B409-11, The 67th JSAP Spring Meeting (2020).
6. H. Masuda, **B. Biswas**, MD S. Islam and K. Kitamura, "Optical Loss Measurement Using an Amplified-Spontaneous-Emission Feedback Circuit with High Improvements in Optical Power Resolution," B-13-7, IEICE Society Conference (2020).
7. H. Masuda, **B. Biswas**, MD S. Islam and K. Kitamura," A Novel Optical Power Measurement Scheme Using an Amplified-Spontaneous-Emission Feedback Circuit with High Improvements in Optical Power Resolution," IEICE Technical Report, OFT-2020-40, pp.17-20 (2020).
8. H. Masuda and **B. Biswas**, "Highly Sensitive and Stable Temperature Sensing Method Using Amplified Spontaneous-Emission Feedback Circuit," 26th Micro-optics Conference (2021) (International Conference with Review). DOI: 10.23919/MOC52031.2021.9598083
9. Hiroji Masuda and **Biswajit Biswas**, "Theoretical Investigation on the Performance of an Amplified-Spontaneous-Emission Feedback Circuit in Optical Power Measurement," OFT-2020-64, pp.38-43, IEICE Technical Report (2021).
10. Hiroji Masuda, **Biswajit Biswas** and Kunihiro Tanaka, "Fiber-Optic Temperature Sensing Method Using an Amplified-Spontaneous-Emission Feedback Circuit," B-13-1, IEICE Society Conference (2021).
11. Kunihiro Tanaka, Hiroji Masuda and **Biswajit Biswas**, "Fiber-Optic Temperature Sensing with Amplified Spontaneous Emission from Erbium-Doped Fiber," The 72nd Annual Meeting of the Chugoku Branch of the Electrical and Information Society (2021).
12. Hiroji Masuda, **Biswajit Biswas** and Kunihiro Tanaka, "Fiber-Optic Temperature Sensing with High Resolution and Stability by Detecting Amplified Spontaneous Emission," OECC (2022). DOI: 10.23919/OECC/PSC53152.2022.9850201
13. Hiroji Masuda, Kunihiro Tanaka, Ryuga Harada, MD Golam Barkatul Abrar, and **Biswajit Biswas**, "Design and Performance of an Amplified Spontaneous-Emission Feedback Circuit for Fiber-Optic Temperature Sensing," IEICE Technical Reports, OFT2022-16, Vol.122, No.162, pp. 50-55 (2022).
14. Golam Barkatul Abrar, Kunihiro Tanaka, Ryuga Harada, **Biswajit Biswas** and Hiroji Masuda, "Parameter Dependence of the Performance of an Amplified Spontaneous-Emission Feedback Circuit," B-13-1, IEICE Society General Conference (2023).
15. Md Golam Barkatul Abrar, **Biswajit Biswas**, Kunihiro Tanaka, Ryuga Harada, Kokoro Kitamura, and Hiroji Masuda, " Amplified-spontaneous-emission feedback circuit technique with high optical power resolutions for multicore-fiber sensing," 7th International Symposium on Extremely Advanced Transmission Technologies- EXAT (2023)

Abstract

Optical power resolution (OPR) is one of the critical factors of an optical power meter in a fiber-optic sensing/measurement system. In the first part of this study, a novel amplified spontaneous-emission feedback circuit (ASEFC) is used in front of a conventional optical power meter to create a fiber-optic sensing technique known as the "ASEFC technique." The technique significantly improves the OPR due to the nonlinearity of the ASEFC, which operates close to the lasing threshold. The characteristics of the OPR using an ASEFC scheme have been experimentally demonstrated. The OPRs were less than 0.14 mdB, and the sensitivity or improvement factor was greater than 67, where mdB stands for milli dB (10^{-3} dB).

A temperature control ASEFC is proposed in the second part of the study with a high-resolution and stable optical power measurement. The optical power of the lights emitted from the two different light sources is measured using the proposed technique with a remote distance of 20 km. The repeatability of the temperature-controlled ASEFC technique with an improved OPR is experimentally evaluated. The small time variations in the optical power of the light sources are accurately measured for one hour, with improvement factors greater than 97. The OPRs are better than 0.10 mdB when the temporal power fluctuation uncertainty of an optical power meter set after the temperature-controlled ASEFC is assumed to be 10 mdB.

Finally, this study experimentally demonstrates the operating bandwidth and dynamic range characteristics of ASEFC. The technique operates successfully in a wide wavelength range of 1530–1560 nm, where the maximum sensitivity is approximately greater than 100. Implementing a temperature-controlled ASEFC technique at a lowest input power level of approximately –5.2 dBm, the small loss variation of a variable optical attenuation has been measured in a remote optical distance of 50 km. When a display resolution of the optical power meter 10 mdB is set after the ASEFC in remote sensing measurement, the improvement factor of the proposed ASEFC measurement technique is larger than 61, and the improved OPR is achieved less than 0.17 mdB.

Table of contents

1. Introduction

1.1 Background

Fiber-optic sensing technology has attracted remarkable attention in optical measurement and communication systems. Fiber-optic sensing technology offers advantages in wide and remote sensing areas, low cost, lightweight construction, improved stability, and accuracy, and various industrial and environmental sensing applications [1-4]. For instance, measuring the gain or loss of any optical devices or components from a remote location in an optical communication system is an ideal example of fiber-optic sensing. Fiber-optic sensors are classified based on their spatial distribution measurand, including point, integrated, distributed, and quasi-distributed. Fiber-optic sensors can be divided into intrinsic and extrinsic sensors based on their nature. Numerous techniques exist for fiber-optic sensing applications, including fiber Bragg gratings, Sagnac interferometry, and Michelson interferometry. Temperature, strain, pressure, refractive index, and displacement are among the most commonly-measured parameters in fiber-optic sensing applications. For example, K. Nakazawa et al. developed a fiber-optic sensor to detect water penetration in underground closers [4]. J.R Zhao et al. proposed a fiber-optic sensor to detect the temperature [11]. Y. Mizuno et al. demonstrated a fiber-optic sensor to detect the refractive index [15]. K. Fukushima et al. proposed a fiber-optic sensor to detect the displacement of an erbium-doped fiber (EDF) laser [17].

The most crucial device to develop/propose such fiber-optic sensors/sensing systems in the field of fiber-optic sensing technology is the optical power meter (PM). A key parameter of this optical power meter is optical power resolution. They are also known as “OPR,” which is the degree of sensitivity of the optical power variation [18-22]. The basic fiber-optic sensing/measurement technique is a photodiode-based optical power meter. The conventional PM comprises an electrical circuit and a photodetector module

(PDM), such as a photodiode (PD). PD-based PMs are widely used because of their excellent performance in low noise, high stability, and high OPR. In most photodiode-based optical sensing applications, the OPR of the PM is expressed in decibels (dB) or %. The typical range of OPR is 0.1 or (0.01 dB or 0.23%) [6, 7, 8, 9]. For example, The OPR is constrained in the conventional measurement system by the PM's polarization dependency and interference noise phenomenon, each with a value between ±0.005 and ±0.015 dB [7].

Previous research by our group proposed a fiber-optic sensing scheme to enhance the sensitivity of OPR. This scheme was achieved using an erbium-doped fiber ring circuit (FRC) [18]. The FRC is a circuit consisting of a gain medium EDF and operates under the laser threshold. As the FRC operates under the laser oscillation condition, it exhibits nonlinearity. The result is a crucial improvement in the sensitivity of FRC-based fiber-optic sensing, by a factor of approximately 32, compared to conventional sensing. Another study conducted by our research group later confirmed the nonlinear characteristics of the FRC experimental method using semiconductor optical amplifiers (SOAs) [19]. In that experiment, the SOA was used as the gain medium of the FRC instead of EDF. The sensitivity of the FRC technique, based on SOA, was enhanced by a factor of around 50. The optically-amplified feedback circuit (OAFC) was named as such. Later, the measurement technique that utilizes the proposed circuit is the amplified-spontaneous-emission feedback circuit (ASEFC) technique.

1.2 Research problems

The proposed sensing scheme by our research group significantly improved the sensitivity in fiber-optic sensing. However, some essential parameters that influence the performance of the FRC or ASEFC, such as output wavelength, loop loss, and others, need to be optimized to improve the technique. The accuracy of the proposed measurement technique and the characteristics of OPR during optical loss measurement needed to be clarified. It is necessary to demonstrate the OPR that is dependent on the conditions, such as the measurement time. The influences of the light sources need during the measurement needed to be clarified. The gain medium of the proposed technique, EDF, has a temperature dependency that significantly impact on the OPR and needs to be optimized. Furthermore, the bandwidth and the dynamic range characteristics of the proposed ASEFC measurement technique require clarification.

1.3 Motivation

In order to improve the OPR of the ASEFC technique, considerable attention has been given to this research as follows.

1. In the first study, an optical measurement technique is proposed after optimizing the performance dependency of the ASEFC. This technique demonstrates the loss measurement of an optical component with a significantly improved OPR compared to the conventional measurement technique. The OPR characteristics of the proposed technique are experimentally clarified by measuring the loss variation of the tested variable optical attenuator (VOA).
2. The second study proposes a temperature-controlled ASEFC to improve OPR and stable optical power measurement technique, where the gain medium of the ASEFC is placed in temperature controlled module. The OPR and repeatability characteristics of the temperature-controlled ASEFC are demonstrated at a remote distance using two light sources. The study shows that the time duration of the accurate measurement of the proposed scheme is improved using the temperature-controlled-ASEFC.
3. Finally, with an improved OPR and temperature-controlled ASEFC, this study focuses on demonstrating the bandwidth characteristics and dynamic range of the ASEFC. Optimizing the dynamic range of the ASEFC technique improves

the remote sensing distance of the optical loss measurement with a high-resolution and wide bandwidth range.

1.4 Significance of this study

The proposed fiber-optic measurement technique with an optimized ASEFC significantly improved the OPR. Further, the OPR characteristic is clarified with better stability by proposing temperature-controlled ASEFC for the first time. The sensitivity and time duration of the loss variation measurement of the proposed technique is improved in this study. In order to clarify the relationship between the input and output power of the ASEFC technique, an equation is confirmed with excellent accuracy and repeatability. The technique successfully demonstrates the gain or loss measurement of the optical components at a remote distance with wide bandwidth characteristics and high dynamic range.

1.5 Scope of this study

Numerous applications, including long-distance and wide-area sensing, environmental sensing, optical device or component loss or gain measurement, and industrial monitoring, may employ our ASEFC scheme. Due to the high sensitivity, better stability, high dynamic range, and wide bandwidth characteristic of ASEFC, the scheme can be implemented in any fiber-optic sensing/measurement applications requiring high OPR. This study demonstrates the ASEFC-based measurement technique within the C-band with a single-mode fiber-optic module. The future scope of the fiber-optic sensing/measurement system can be introduced by extending the operating band to C plus L-band utilizing the ASEFC technique within a multi-mode, multi-core fiber-optic system.

1.6 Outline of the study

The proposed study suggests a fiber-optic sensing system based on ASEFC that improves the resolution of optical power.

The first section of the study is entitled “Introduction”. This section presents the background, research problem, motivation, significance, and scope of the study.

The second section of this study is called “Fundamentals”. This section provides an overview of the fundamental design and features of ASEFC. Besides, experimental and numerical simulation methods explore the ASEFC-based measurement technique's performance dependence. This chapter also covers practical applications of the ASEFC measurement scheme, such as sensing variations in loss and remote temperature.

Chapters three, four, and five of this thesis dissertation are vital, each featuring a significant topic published in peer-reviewed journals. Every chapter includes a brief overview, a description of the experimental setup, results, a discussion, and a conclusion.

Chapter three, entitled “ASEFC Scheme for Optical Power Sensing,” explains the ASEFC-based fiber-optic measurement scheme that significantly enhances optical power resolution.

Chapter four is titled “Temperature-controlled ASEFC with improved OPR for Optical Power Sensing.” This chapter presents a temperature-controlled ASEFC scheme for optical power sensing. Two types of pump light sources are employed to showcase this sensing technique.

Chapter Five is titled “Bandwidth and Dynamic Range Characteristics of ASEFC.” The chapter elaborates on the bandwidth and dynamic range of the measurement technique. The chapter also explicates a temperature-controlled ASEFC scheme for remote optical power sensing. Additionally,

The summary of the thesis and future issues are presented in Chapters Six and Seven.

All references to this thesis dissertation are located in Chapter Eight.

2. Fundamentals

2.1 Basic configuration of ASEFC

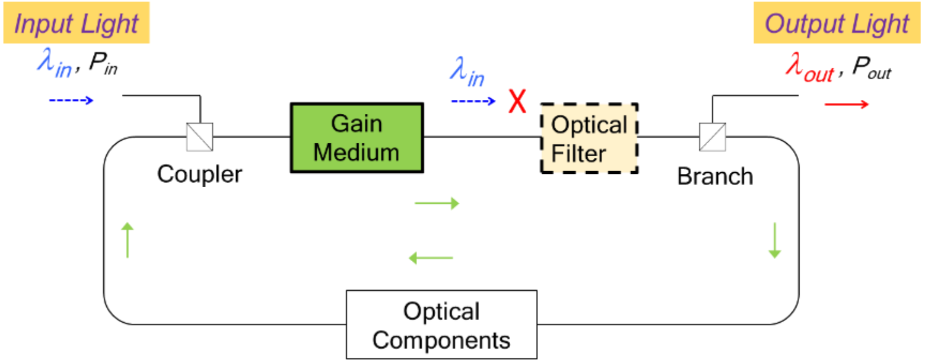

Fig. 2.1 Basic configuration of ASEFC. (Copyright(C) 2020 IEICE, [47] Fig. 2).

Fig. 2.1 shows the basic configuration of the ASEFC. Amplified Spontaneous Emission (ASE) is feedback into the gain medium around the operating point of the laser threshold [24-26]. The wavelength of the input light is the signal or pump wavelength of the gain medium. Since lasers typically operate in the region well above the lasing threshold, the ASEFC differs from them in theory. In ASEFC, the output light's wavelength is different from the input light's. In contrast to an optical amplifier, which operates when the two wavelengths coincide, this operation is different in theory. The ASEFC technique improves the OPR by factors of the order of 10 to 100 by utilizing the nonlinear relationship between input and output powers measured in dBm [17, 18, 19, 20].

2.2 Conventional technology vs ASEFC-based technology

A photo-diode-based optoelectronic circuit was employed in a conventional method to determine and limit the resolution in the systems [6-9]. The resolution is often measured in dB units with values around 0.1 or 0.01 dB [7, 8, 10, 11]. Our proposed ASEFC operates in or close to the laser oscillation condition and comprises of a gain medium and an optical feedback channel. We have achieved an improvement factor (IF) of approximately 10 to 100 depending on the experimental conditions.

In this study of optical power sensing, three system configurations are shown in Fig. 2.2. The initial configuration of a typical conventional system is shown in Fig. 2.2(a). The second arrangement for a traditional method utilizing an optical amplifier is depicted in Fig. 2.2(b). The third configuration for our proposed ASEFC method is shown in Fig. 2.2(c). The three methods each consist of a light source (LS), a photo-diode module (PDM), and a device under test (DUT). A photo-diode is present in the PDM, and an electrical circuit follows it. The DUT, which can be either an optical amplifier or a passive optical component, is an optical gain medium. In the first configuration, the photodetector (PD) of the optical power measuring system is the PDM itself. The input and output from the DUT are the light emitted from the LS launched into the PDM. The wavelength of the light is denoted as λ. In contrast, the second configuration of the PD consists of a PDM and an optical amplifier (OA) placed in front of the PDM. The input of ASEFC was the light emitted from the DUT, and the OA amplified the input. In addition, the third configuration of the PD includes an ASEFC placed in front of the PDM. The emitted light from the input goes through the DUT and is received by the ASEFC. P_{in} and P_{out} in dBm units are denoted as the input and output light powers for the OA and ASEFC, respectively.

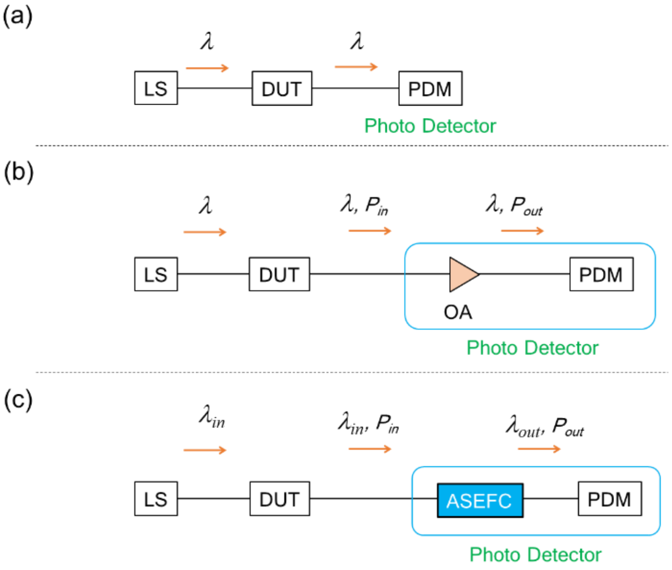

Fig. 2.2 System configurations.(a) Conventional Scheme, (b) Conventional Scheme with an optical amplifier (OA), (c) ASEFC Scheme. (Copyright(C) 2020 IEICE, [47] Fig. 1).

The input and output wavelengths of the lights are denoted as λ_{in} and λ_{out}, respectively. The wavelength emitted from the output light of the OA equals that of the input light in the second scheme, whereas λ_{out} is different from λ_{in} in the third scheme. Despite using an OA in front of the PDM in the second method, the resolution of the PD in dB units is constrained by the PDM if the signal-to-noise ratio of the light identified by the PDM in the electrical domain is sufficiently high, as shown in the following illustration. Let P_{k0}, where k=in or out, respectively, be the optical power of the input and output lights of both the OA and ASEFC. Let P_{k0} and P_{k}, represent the incremental power variation in mW and dBm units, respectively. The expression for ΔP_{k} is. $\Delta P_{\mathrm{k}}=(10/\ln 10)\Delta P_{\mathrm{k0}}/P_{\mathrm{k0}}$. As a result, ΔP_{k} is inversely proportional to the relative accuracy of $\Delta P_{\mathrm{k0}}/P_{\mathrm{k0}}$. The resolutions, or ΔP_{k}, typically have values in the range of 0.1 or 0.01 dB [6]. Because of the relationships $P_{\mathrm{out0}}= GP_{\mathrm{in0}}$ and $\Delta P_{\mathrm{out0}}= G\Delta P_{\mathrm{in0}}$ where G is the amplifier gain, if we employ an OA in the case of the second scheme (Fig. 2.2 (b)), the relative accuracy of the output light $\Delta P_{\mathrm{out0}}/P_{\mathrm{out0}}$ equals the relative accuracy of the input light $\Delta P_{\mathrm{in0}}/P_{\mathrm{in0}}$. So, $\Delta P_{\mathrm{out}}=\Delta P_{\mathrm{in}}$." This indicates that the resolution has remained the same. On the other hand, as seen in the following, we can establish the following relation utilizing the ASEFC and improve the resolution of PD. The ratio (IF = S): $S= \Delta P_{\mathrm{out}}/\Delta P_{\mathrm{in}}$ gives the improvement factor IF. Keep in mind that IF S of the conventional scheme using the OA is 1.

2.3 Basic parts of ASEFC

The experimental setup of our proposed ASEFC is depicted in Fig. 2.3. As the source of the system's input light, the pump light produced by erbium-doped fiber (EDF) was used. As in the examples [20-22], the input light might be selected to function as the signal light of the EDF. The input light, or pump light, was produced by a pump light source (PLS) such as a Fabry–Perot laser diode module or fiber Bragg grating laser diode module. In this case, input light had a wavelength of approximately 1470 nm. A constant current drives the PLS, and an optical variable attenuator (VOA) is fitted after the PLS. This VOA adjusts the amount of optical power fed into the EDF input. A branch fiber module (BR) is used to monitor the power of the input light after it has been branched, and this power is then measured by an optical power meter (PM1). An EDF is used in the ASEFC as the gain medium, and a fiber ring structure is used for the feedback path [18]. An optical isolator, or an ISO, is installed on both sides of the EDF to exclude light traveling in the anti-clockwise direction and any residual reflection. An optical coupler (CP) connects the input light to the fiber ring circuit, and a pump rejection optical filter (PR) eliminates any remaining pump emitted from the EDF. Both of these steps take place in the same optical cavity. Installing an optical bandpass filter, an OBPF comes after the EDF component. After the OBPF, a polarization controller (PC) is installed. A branch fiber module (BR) is also installed after the PC. An optical attenuator, an ATT, is installed after the BR in the loop.

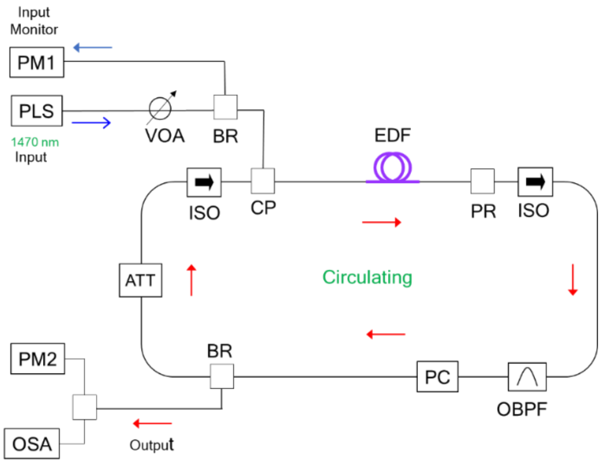

Fig. 2.3 ASEFC configuration. (Copyright(C) 2019 IEICE, [37] Fig. 1).

The obtained light is branched by the BR in the loop as the output light of the ASEFC. The optical power and wavelength of the output light are measured by an optical power meter (PM2) and an optical spectrum analyzer (OSA), respectively, where PM2 and the OSA are set after the BR in the loop. The center wavelength of the OBPF (λ_c) changed to 1548, 1558 and 1568 nm [37]. The input and output light powers for the ASEFC are labeled as P_{in} and P_{out} in dBm units, respectively.

Three major sections of ASEFC are

1. Input monitor section.
2. Feedback section.
3. Output monitor section.

2.3.1 Input monitor section

The input monitor section, labeled green in Fig. 2.4, is the input section of the ASEFC. A laser diode module is used as a pump light of ASEFC. The ~1470 and ~1455 nm wavelength was used as an input light for Fabry-Perot and fiber Bragg grating type laser diode module [28]. Depending on the experimental requirement, sometimes an optical variable attenuator (VOA) is located at the PLS's rear portion and used to adjust the input optical power. An optical power meter (PM1) and PLS are connected through a branch fiber module (BR) to monitor the power of the input light.

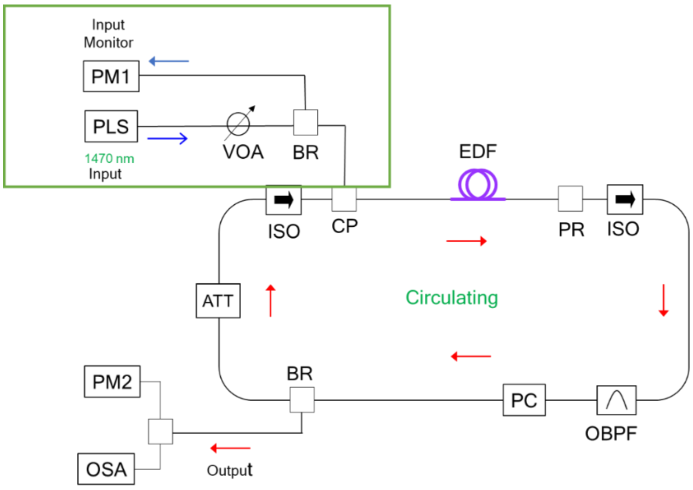

Fig. 2.4 Input monitor section of ASEFC. (Copyright(C) 2019 IEICE, [37] Fig. 1).

2.3.2 Feedback section

The section for feedback is labelled green in Fig. 2.5.The ASEFC uses an EDF as its gain medium and has a fiber ring-shaped feedback path. The input and feedback parts of the ASEFC are connected by an optical coupler (CP). The residual pump was eliminated when the input light was attached to the fiber ring circuit using a CP and a pump rejection optical filter (PR). Each side of the EDF has an optical isolator (ISO) to stop light from propagating counterclockwise and residual reflection. After the EDF section, an optical band pass filter (OBPF) is set and connects the polarization controller (PC). In addition, a second branch fiber module (BR) is installed following the PC. After the BR is in the loop, an optical attenuator (ATT) is placed.

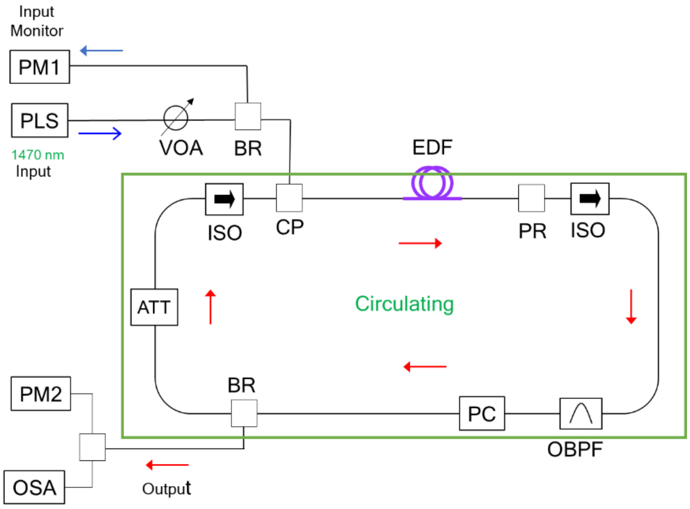

Fig. 2.5 Feedback section of ASEFC. (Copyright(C) 2019 IEICE, [37] Fig. 1).

2.3.3 Output monitor section

The output monitor section indicated in Fig. 2.6 is labelled green. The light obtained by the branch BR in the loop is the output light of the ASEFC. The optical power and wavelength of the output light are measured by an optical power meter (PM2) and an optical spectrum analyzer (OSA), respectively, where PM2 and the OSA are set after the BR in the loop. The center wavelength of the OBPF (λ_c) followed the output wavelength of the ASEFC. The input and output light powers for the ASEFC were labelled as P_{in} and P_{out} in dBm units, respectively.

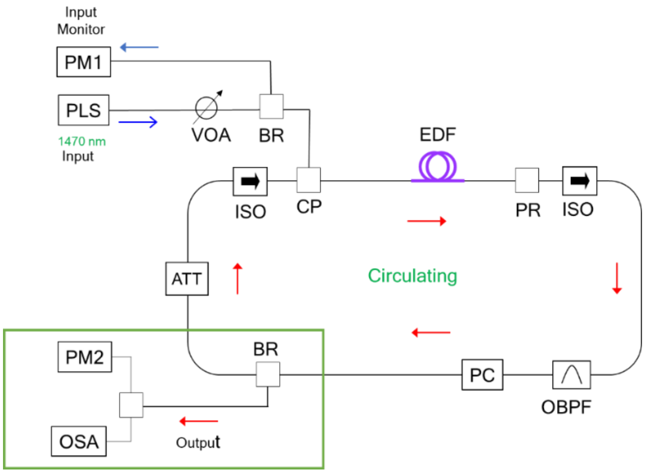

Fig.2.6 Output monitor section of ASEFC. (Copyright(C) 2019 IEICE, [37] Fig. 1).

2.4 Slope comparison (conventional scheme vs ASEFC scheme)

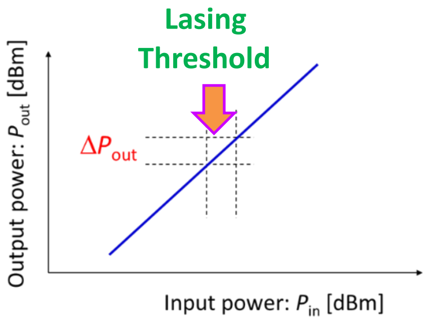

Fig. 2.7 (a) Output power as function of input power in conventional scheme. (Copyright(C) 2020 IEICE, [47] Fig. 3(a)).

Conventional scheme, **"Slope"** $S \equiv \frac{\Delta P_{\mathrm{out}}}{\Delta P_{\mathrm{in}}} = 1$

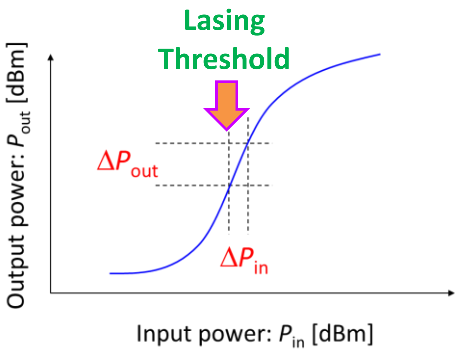

Fig. 2.7 (b) Output power as function of input power in ASEFC scheme. (Copyright(C) 2020 IEICE, [47] Fig. 3(b)).

ASEFC scheme, **"Slope"** $S \equiv \frac{\Delta P_{\mathrm{out}}}{\Delta P_{\mathrm{in}}} \gg 1$

Fig. 2.7(a) and (b) show the slope characteristics of the conventional optical amplifier and ASEFC scheme, respectively. In conventional optical amplifier scheme, the output power P_{out} is a linear function of the input power P_{in} and the slope S equals 1. On the other hand, P_{out} is a nonlinear function of $P_{\text{in},}$ and the slope S becomes significantly more prominent than 1 when the ASEFC operates around the laser oscillation threshold.

2.5 Wavelength dependence of ASEFC

In this study, the output wavelength dependence of the ASEFC is investigated for a multi-wavelength optical sensing system. Similar to the configuration of Fig. 2.3, the center wavelength of the OBPF (λ_c) changed to 1548, 1553, 1558, 1563 and 1568 nm [38]. In Fig. 2.8, (a) shows P_{out} as a function of P_{in}, (b) $S_{\max}$ shows vs P_{out}, (c) shows $S_{\max}$ vs λ_c . In this study, $S_{\max}$ was achieved 418 at the optimized wavelength of 1553 nm.

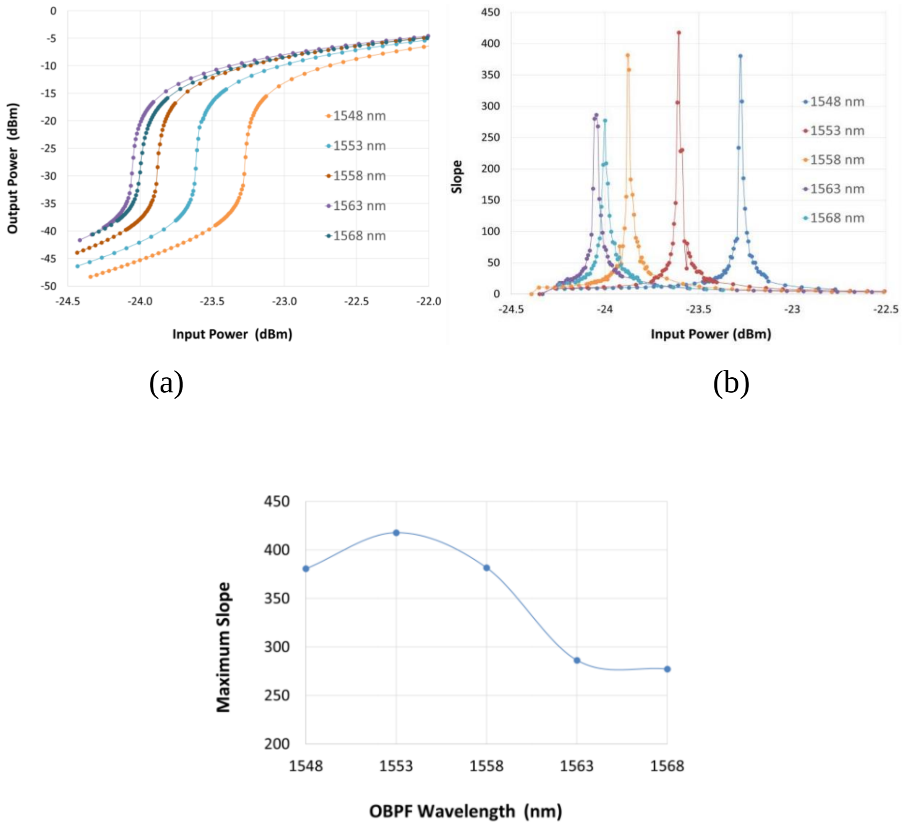

(a) (b)

(c)

Fig. 2.8 a) Output power as a function of input power, b) Slope as function of input Power and c) Maximum Slope as a function of OBPF wavelength. (Copyright(C) 2019 HISS, [38] Fig. 2, 3, 4).

2.6 Numerical simulation on the performance of an ASEFC in optical-power sensing applications

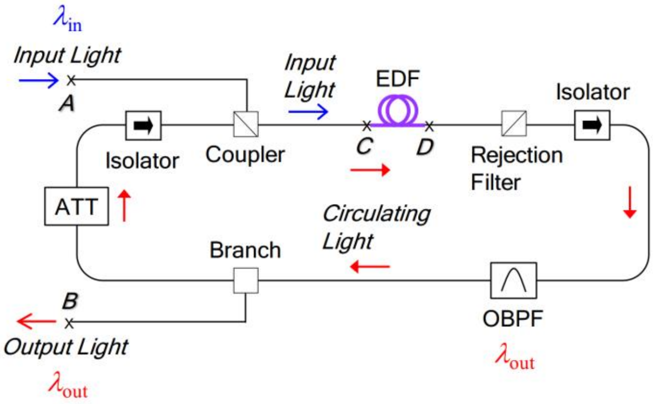

Fig. 2.9 Configuration of an ASEFC. (Copyright(C) 2021 IEICE, [49] Fig. 2).

In this study, a theoretical investigation was presented including modeling and numerical simulation of the ASEFC [49]. Fig. 2.9 shows the ASEFC configuration for modeling and numerical simulation. In Fig. 2.10, the input and output signal lights, the input and output pump lights, and the forward and backward ASE lights (F-ASE and B-ASE) are schematically depicted in the light propagation in the EDF. Additionally shown is the spontaneous emission light that the EDF emits laterally. For the sake of simplicity, the backward ASE light is not considered in the modeling that follows because preliminary numerical simulation results show that its impact on the effectiveness of the ASEFC scheme is the minimum [105].

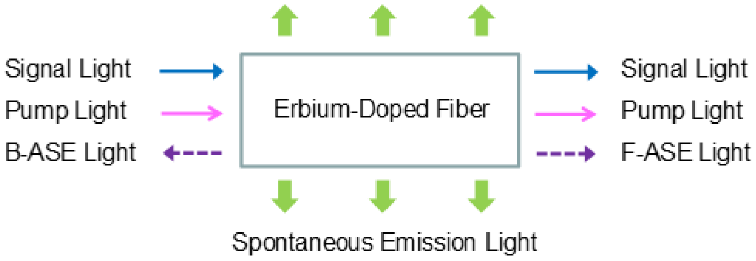

Fig. 2.10 Input and output lights of an erbium-doped fiber. (Copyright(C) 2021 IEICE, [49] Fig. 3).

Let $P_{\text{in-cir}}$ and $P_{\text{out-cir}}$, at Points C and D, respectively, be the input and output circulating light powers in mW. Let $P_{\text{ASE-tot}}$ and $P_{\text{ASE-BP}}$, respectively, stand for the total ASE power and the spectrally filtered ASE power. The ASE spectrum components at wavelengths between 1520 and 1605 nm are taken into account when calculating the total ASE power. In the OBPF bandwidth ($\Delta\lambda$), the ASE light with a power of $P_{\text{ASE-BP}}$ and the output circulating light with a power of $P_{\text{out-cir}}$ from the EDF at Point-*D* are both fed back into the EDF at Point-*C* via the feedback loop from Point-*D* to -*C*. Let *G* and *L*, respectively, represent the EDF's gain and the feedback loop's loss from Point-*D* to -*C*. Additionally, let L_{in} and L_{out}, respectively, represent the optical losses between Points *A* and *C* and between Points *B* and *D*. The following equations from Eq. (2.1) to (2.4) and Eqs. (2.5) and (2.6) provide a number of relations from the relationships mentioned above. Both the feedback loop of the ASEFC and the differential equations of the lights propagating in the EDF were simultaneously and numerically solved. The center transmission wavelength of the OBPF, the flat gain of the EDF, and the loop loss from Point-*D* to -*C* were all set to 1550 nm, 20 dB, and 10 dB, respectively, in the numerical simulation. When the EDF displays a flat gain spectrum in the C-band [106], take note that the gain at 1550 nm is 20 dB. The light used as an input had a wavelength of 1470 nm. For simplicity, L_{in} and L_{out} were coupling losses, which set to zero (0 dB).

$$P_{\text{out}-\text{EDF}} = P_{\text{out}-\text{cir}} + P_{\text{ASE}-\text{tot}} \quad (2.1)$$
$$P_{\text{out}-\text{BP}} = P_{\text{out}-\text{cir}} + P_{\text{ASE}-\text{BP}} \quad (2.2)$$
$$P_{\text{in}-\text{cir}} = LP_{\text{out}-\text{BP}} \quad (2.3)$$
$$P_{\text{out}-\text{cir}} = GP_{\text{in}-\text{cir}} \quad (2.4)$$
$$P_{\text{in}-\text{mW}}L_{\text{in}} = P_{\text{in}-\text{EDF}} \quad (2.5)$$
$$P_{\text{out}-\text{mW}} = L_{\text{out}}P_{\text{out}-\text{BP}} \quad (2.6)$$

Fig. 2.11 shows the input (P_{in}) and output (P_{out}) relation (a) and the slope (*S*) characteristics (b) at the bandwidth $\Delta\lambda$ of 1, 0.1, and 0.01 nm. From Fig. 2.11 (b), the slope *S* increases as the bandwidth $\Delta\lambda$ decreases. This is because the ASE filtering effect increases as $\Delta\lambda$ decreases.

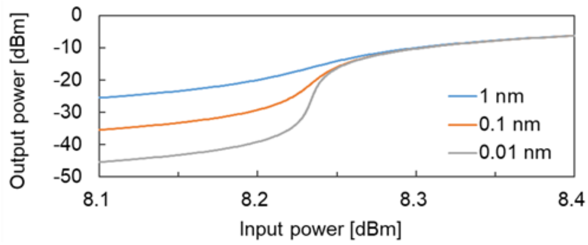

(a)

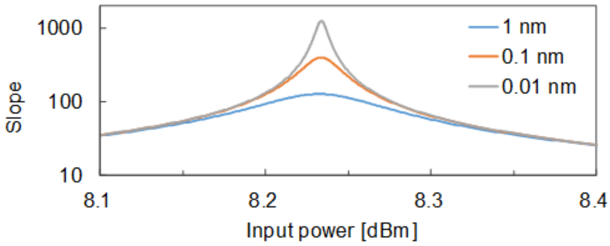

(b)

Fig. 2.11 The input and output relation (a) and the slope characteristics (b) of the ASEFC. (Copyright(C) 2021 IEICE, [49] Fig. 4).

Then, $\Delta\lambda$ dependence of S is shown in Fig. 2.12. From the figure, S increases as $\Delta\lambda$ decreases in the $\Delta\lambda$ range from 0.01 to 1 nm. For example, S are 127, 400, and 1261 at $\Delta\lambda$ of 1, 0.1, and 0.01 nm, respectively.

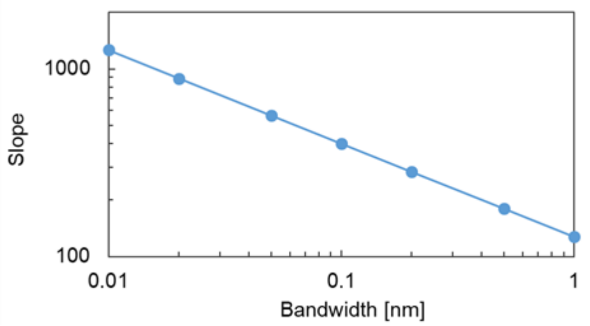

Fig. 2.12 OBPF-bandwidth dependence of the slope of the ASEFC. (Copyright(C) 2021 IEICE, [49] Fig. 5).

Fig. 2.13 shows the gain G in dB unit, the EDF output power of the circulating light $P_{\text{out-cir}}$, the ASE power output from the EDF evaluated after the OBPF $P_{\text{ASE-BP}}$, and the sum of the powers $P_{\text{out-cir}}$ and $P_{\text{ASE-BP}}$ ($P_{\text{out-BP}} = P_{\text{out-cir}} + P_{\text{ASE-BP}}$, see Eq. 2.2) in dBm unit as a function of the input power (pump light power) P_{in} in dBm unit at the OBPF bandwidth $\Delta\lambda$ of 1 nm and 0.01 nm.

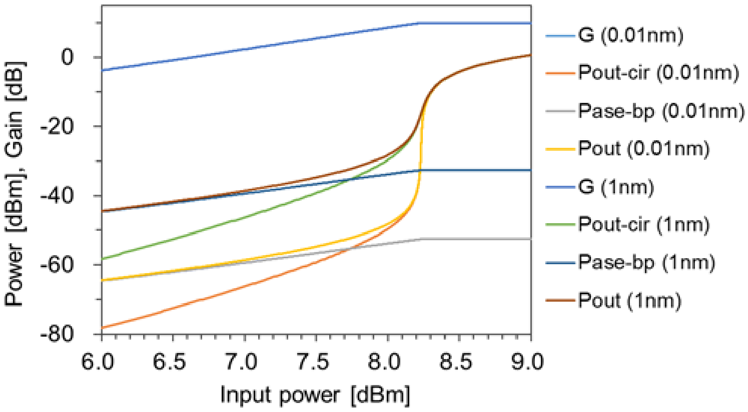

Fig. 2.13 Characteristics of the gain and optical powers of the ASEFC. (Copyright(C) 2021 IEICE, [49] Fig. 6).

Fig. 2.14 shows the difference of powers (ΔP) $P_{\text{out-cir}}$ and $P_{\text{ASE-BP}}$, $\Delta P = P_{\text{out-cir}} - P_{\text{ASE-BP}}$, as a function of P_{in} at $\Delta\lambda$ of 1 nm, 0.1 nm, and 0.01 nm. In the operation region where the gain G in dB is far smaller than the loss L in dB (10 dB), the power difference ΔP has values less than ~0dB. ΔP increases rapidly when the input power P_{in} approaches the laser threshold power of ~8.2 dBm. In the region of P_{in} much larger the threshold, ΔP has values more than ~20dB, and the differences in ΔP among $\Delta\lambda$ of 1 nm, 0.1 nm, and 0.01 nm is inversely proportional to $\Delta\lambda$ in dB units so that ΔP at $\Delta\lambda$ of 0.1 nm is 10 dB larger than ΔP at $\Delta\lambda$ of 1 nm, and so on.

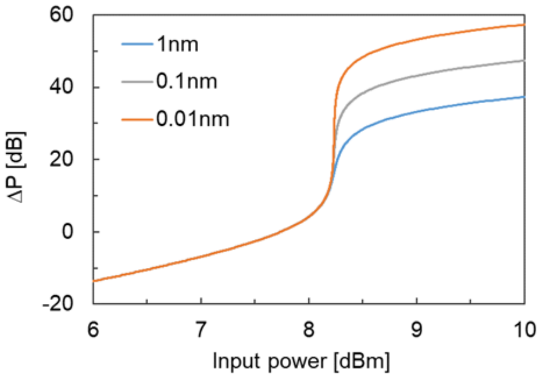

Fig. 2.14 Difference of powers between the circulating light output and the filtered ASE output. Copyright(C) 2021 IEICE, [49] Fig. 7).

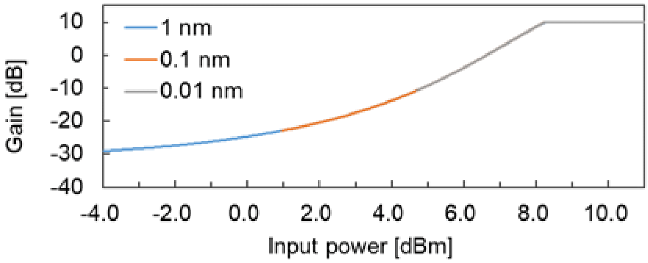

(a)

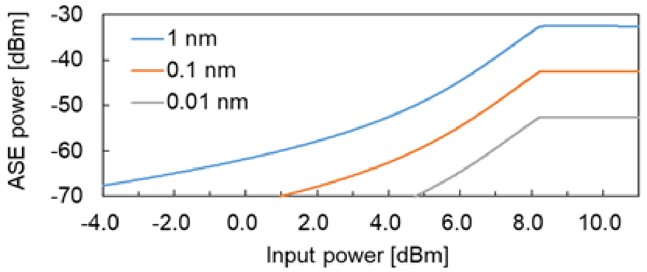

(b)

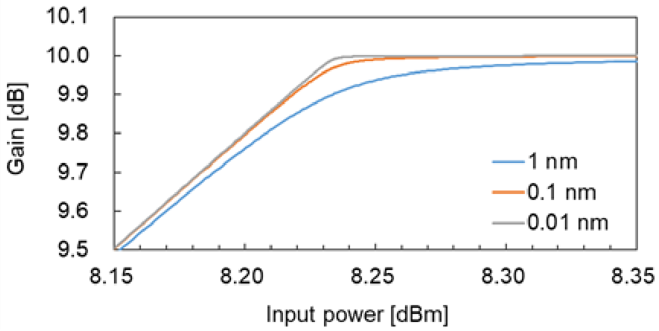

(c)

Fig. 2.15 Gain and ASE power characteristics. Copyright(C) 2021 IEICE, [49] Fig. 8).

Gain and ASE power characteristics are shown in Fig. 2.15. Fig. 2.15(a) shows the gain G in dB unit as a function of P_{in} from −4 dBm to 11 dBm in the case of $\Delta\lambda$ of 1 nm, 0.1 nm, and 0.01 nm. Fig. 2.15(b) also shows the ASE power $P_{\mathrm{ASE\text{-}BP}}$ in dBm unit as a function of P_{in} from −4 dBm to 11 dBm in the case of $\Delta\lambda$ of 1 nm, 0.1 nm, and 0.01 nm. Moreover, Fig. 2.15(c) shows G as a function of P_{in} from 8.15 dBm to 8.35 dBm where the range is around the laser threshold input power ($P_{\mathrm{in\text{-}th}}$) of ~8.23 dBm. From Figs. 2.15(a) and (c), the gains of the three cases of $\Delta\lambda$ of 1 nm, 0.1 nm, and 0.01 nm almost coincide except for the power range around $P_{\mathrm{in\text{-}th}}$. The gain G and ASE power $P_{\mathrm{ASE\text{-}BP}}$ are almost constant in the input power range far above $P_{\mathrm{in\text{-}th}}$. $P_{\mathrm{ASE\text{-}BP}}$ in mW unit is approximately proportional to the gain with no dimension G and the fictitious input photon number in the EDF [106]. The fictitious input photon number is estimated to be almost constant near the threshold power $P_{\mathrm{in\text{-}th}}$ so that $P_{\mathrm{ASE\text{-}BP}}$ in mW unit is approximately proportional to the gain with no dimension G as is shown in Figs. 2.15(a) and (b). From

Fig. 2.15(c), G in dB unit approaches to the loss L in dB unit (10 dB) with smaller variation in P_{in} when the OBPF bandwidth $\Delta\lambda$ becomes smaller from 1 nm to 0.01 nm.

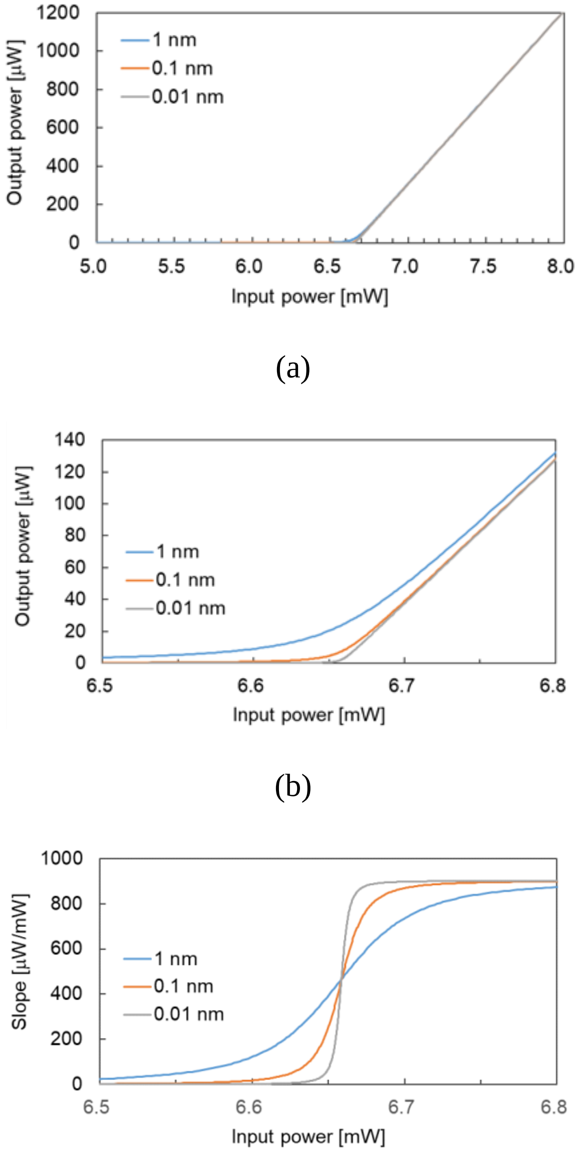

(a)

(b)

(c)

Fig. 2.16 The input and output power characteristics in mW/µW unit. Copyright(C) 2021 IEICE, [49] Fig. 9).

Fig. 2.16 shows the input and output power (P_{in} and P_{out}) characteristics in mW/µW unit in the cases of $\Delta\lambda$ of 1 nm, 0.1 nm, and 0.01 nm. Figs. 2.16(a) and (b) show P_{out} in µW unit as a function of Pin in mW unit in the range of P_{in} from 5 to 8 mW and from 6.5 to 6.8 mW, respectively. From the detailed plots of P_{out} versus P_{in} curves in Fig. 2.16(b), the laser threshold power $P_{\mathrm{in\text{-}th}}$ is 6.66 mW. On the other hand, Fig. 2.16(c) shows the slope of the curves of P_{out} versus P_{in} in the unit of µW/mW (S_{m}W), where the slope S_{m}W is defined as $S_{\mathrm{mW}} \equiv \mathrm{d}P_{\mathrm{out-mW}}/\mathrm{d}P_{\mathrm{in-mW}} \cdot 1000$. From Fig. 2.16(c), we can confirm that S_{m}W monotonically increases with the input power $P_{\text{in-mW}}$. This is apparently different from the case of the slope S where the input and output powers, P_{in} and P_{out}, are measured in dBm unit. Note that each curve of S shows a peak around the laser threshold $P_{\text{in-th}}$ as shown in Fig. 2.11(b).

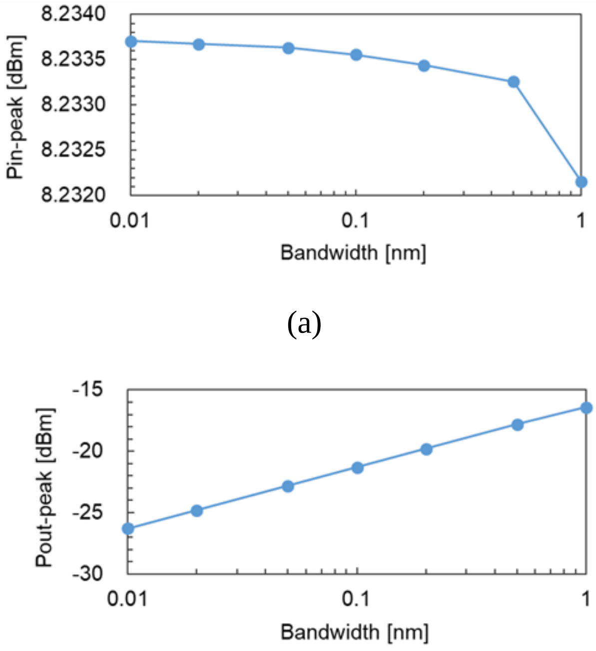

(a)

(b)

Fig. 2.17 The peak input and output powers. Copyright(C) 2021 IEICE, [49] Fig. 10).

We have derived the input power at which the slope S has a maximum value, peak value, in each curve from Fig. 2.11. The input power is labeled as $P_{\text{in-peak}}$. The output power at which the slope S has a peak value is also derived and is labeled as $P_{\text{out-peak}}$. Figs. 2.17(a) and (b) show the input and output powers, $P_{\text{in-peak}}$ and $P_{\text{out-peak}}$, as a function of the OBPF bandwidth $\Delta\lambda$ from 0.01 to 1 nm. The variation in $P_{\text{in-peak}}$ with $\Delta\lambda$ is small to within 0.002 dB from 8.232 to 8.234 dBm. On the other hand, $P_{\text{out-peak}}$ varies from −26.3 dBm at $\Delta\lambda$ of 0.01 nm to −16.4 dBm at $\Delta\lambda$ of 1 nm. Such a power of $P_{\text{out-peak}}$ can be easily measured by a photo-diode module set after the ASEFC. Note that if we assume a coupling loss L_{out} defined by Eq. (2.6) of ~5 dB, $P_{\text{out-peak}}$ decreases by L_{out} of ~5 dB.

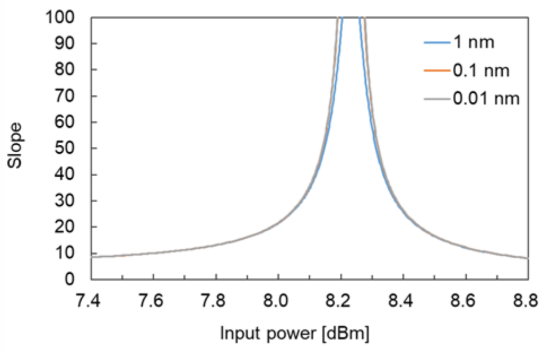

(a)

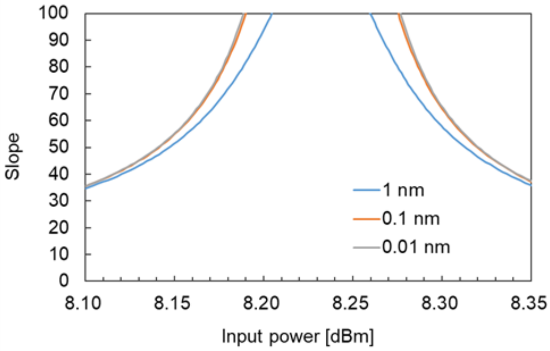

(b)

Fig. 2.18 Input power bandwidth characteristics. Copyright(C) 2021 IEICE, [49] Fig. 11).

Fig. 2.18 shows the slope S in the range less than 100 as a function of P_{in} in the cases of $\Delta\lambda$ of 1 nm, 0.1 nm, and 0.01 nm, where S has values larger than ~10. From Fig. 2.19 (a), the input power bandwidth (ΔP_{in}) in which S is larger than 10 is ~1.09 dB from P_{in} ~7.60 dBm to P_{in} ~8.69 dBm for all the cases of $\Delta\lambda$ of 1 nm, 0.1 nm, and 0.01 nm. In the same way, from Fig. 2.19(b), ΔP_{in} in which S is larger than 100 is ~0.06 dB from P_{in} ~8.20 dBm to P_{in} ~8.26 dBm at $\Delta\lambda$ of 1 nm. Moreover, ΔP_{in} in which S is larger than 100 is ~0.09 dB from P_{in} ~8.19 dBm to P_{in} ~8.28 dBm at $\Delta\lambda$ of 0.1 nm, and ~0.09 dB from P_{in} ~8.19 dBm to P_{in} ~8.28 dBm at $\Delta\lambda$ of 0.01 nm. Thus, the input power bandwidth ΔP_{in} has an order of ~1 dB or ~0.1 dB when the slope S is larger than 10 and 100, respectively. Therefore, the ASEFC scheme is considered to be effective for measuring a small variation of optical power.

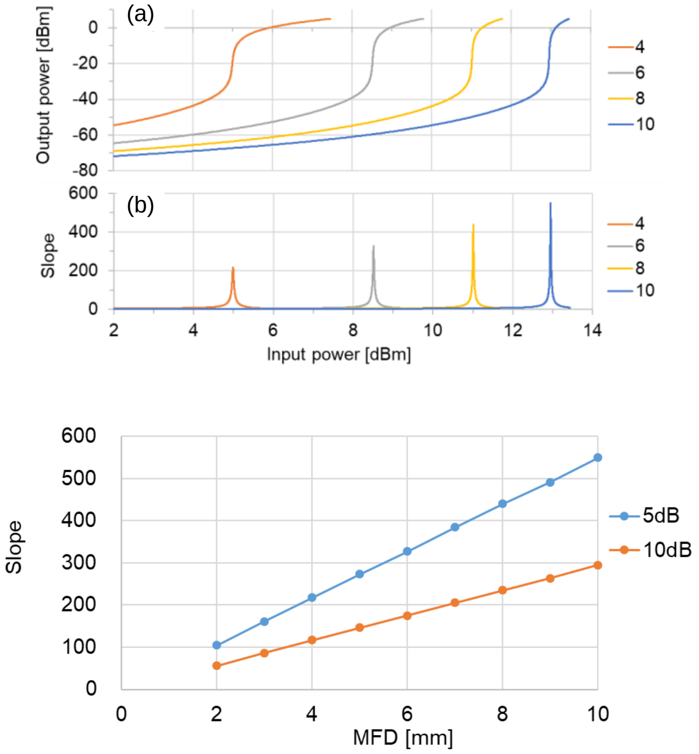

(C)

Fig. 2.19 (a) The output power and (b) the slope as a function of the input power at MFD of 4, 6, 8, 10 μm and (c) Slope as a function of the MFD. (Copyright(C) 2021 IEICE, [40] Fig. 2,3).

In this study, the performance of ASEFC was affected by the fiber parameter, which is the mode-field diameter (MFD) of the EDF [40]. Additionally, the EDF's flat gain and loop loss (L) were set to 25 dB and 5 dB, respectively. As illustrated in Fig. 2.19 (a), the MFD was set to be 4, 6, 8, and 10 μm, with the maximum slope (S_{max}) being 217, 327, 440, and 549, respectively. The peak input power at which the slope S shows a peak value increases with the MFD. S also increases with the MFD. In Fig. 2.19 (a) and (b), the maximum slopes S_{max} of Fig. 2.19 (c) are depicted as a function of the MFD. Along with the instance of L = 5 dB, the simulation results for the case of L = 10 dB are displayed. According to Fig. 2.19 (c), under the measured conditions, S_{max} grows practically linearly with the MFD.

2.7 Temperature sensing using ASEFC

Fiber-optic sensing has received a lot of interest in research and development for various applications, including industrial monitoring and underwater monitoring, among others. [1-4, 57-72]. A temperature sensing technique was proposed by implementing the novel ASEFC technique. Using the temperature dependence of the EDF medium, this fiber-optic technique successfully measurement the temperature.

For example, N. Kagi, et al., The gain in erbium-doped fibers between -20 and +85 °C is discussed in relation to temperature [74]. Z. Yin et al., Based on beat frequency demodulation technology, a novel multi-longitudinal-mode fiber ring laser temperature sensor is presented, and the beat frequency between any two modes changes linearly with temperature. [76]. Jia Shi, et al., for high-resolution measurement, a general technique based on fiber ring laser (FRL) intracavity sensing is proposed, and an experimentally proven high-resolution temperature sensing system is presented. [77]. W. L. BARNES, et al., for the $^4I_{13/2}$- $^4I_{15/2}$ transition a detailed measurement of the emission and absorption cross sections of Er^{3+} doped fibers is presented [78]. M. Yamada, et al., It has been reported that 1.48 μm pumping is more sensitive to temperature than 0.98 μm pumping [79]. E. Desurvire, et al., According to this study, pumps with narrow linewidths and sources for broadband, multimode laser diode pumps should produce equivalent gain performance [81].M. Shimizu, et al., The optical gain for Er-doped silica core single-mode fiber amplifiers with various Er concentrations pumped by 1.48 µm wavelength laser diodes is studied, and the optical amplification characteristics show that the optical gain strongly depends on Er concentration [83].N. Kagi, et al., A 1.48 μm laser diode was used to pump an erbium-doped fiber amplifier, which resulted in a gain coefficient of 3.8 dB/mW [84].T. Pfeiffer, et al., The transverse extension of mode fields and dopant distribution are taken into account in a proposed analytical description of the gain of an erbium-doped fiber amplifier [85].S. L. Hansen, et al., A very high gain of 51 dB is reported in a single Er-doped fiber, and significant amplified Rayleigh backscattering is also observed [86].G. A. Ball, et al., The performance of single- and multipoint active fiber sensors is demonstrate for strain and temperature measurements [88]. G. A. Ball, et al., For the spectral reflectivity of an intracore Bragg phase grating in an amplifying fiber, a closed-form solution is obtained through coupled mode theory and used to design single-mode fiber lasers [89].J. Shi et al., a temperature self-correcting high-resolution refractive index (RI) sensor is demonstrated employing intracavity intensity-modulated sensing in a fiber ring laser, and the resolution of the fiber laser sensor is achieved 2 × 10 -10 RIU with the signal-to-noise ratio more than 55 dB [94]. C. -L. Lee, et al., For the first time, an innovative and ultra-compact hollow core fiber (HCF) end face-based air-gap fiber Fabry-Pérot interferometer (AG-FFPI) is investigated in this study. The suggested device displays an interference fringe wavelength shift that reflects temperature sensitivity, which is equivalent to sensitivity to a change in cavity length [95]. L. Liang, et al., With a sensitivity of 10.8 pm/°C in the temperature range of 8 °C to 80 °C, a novel refractive index (RI) and temperature all-fiber ring laser sensor based on STCS fiber structure is proposed [96]. C. Spiegelberg, et al., a compact integrated fiber laser was present with more than 200 mW of output power [98]. F. Farahi, et al., Numerous physical measurements have demonstrated the sensitivity of interferometric sensors that use optical fibers as a transduction medium [99].J. Shi et al., A fiber ring laser-based temperature sensor with a reflective Sagnac loop is suggested [97]. H. Li, et al., On the basis of polarization-sensitive optical frequency domain reflectometry (OFDR), a distributed temperature sensor (DTS) with centimeter-level spatial resolution is proposed [100]. T. Kurashima, et al., the brillouin gain spectra of two 250 m long single-mode fibers with GeO/sub 2 doped core/pure-silica cladding and pure-silica core/F-doped cladding were measured at temperatures region from -40 to +60 ° C C and at a wavelength of 1.32 μm, [101]. Y. Zhang, et al., On the basis of a bent single mode-multimode-single mode (SMS) fiber layout fixed to a polymer plate frame, a straightforward temperature sensor is proposed with sensing range from 51 to 65 ° C and sensitivity of 6.5 nm/ ° C[103]. Y.

Zhao, et al., A novel temperature sensor based on up-taper and single mode-multimode fiber can achieve the temperature sensitivity of 89.42 pm/°C at the temperature range of 20 °C-80 °C [104].

The system configuration using the proposed ASEFC-TS is shown in Fig. 2.20 [40, 48]. The pump light source of the EDF, which is a gain medium for the ASEFC, is an input light source (LS) with a wavelength of 1470 nm. A 20-km single-mode fiber (SMF) remotely launches the pump light into the ASEFC. The optical band-pass filter (OBPF) with a central wavelength of 1558 nm is used in the feedback loop to feed the light that exited the EDF back into it. A 3-dB fiber coupler branches off a portion of the loop's circulating light, which is then detected by a photodetector (PD) through a 20-km SMF. The temperature control module (T-Control Module) was used to implement the EDF. A temperature controller (T-Controller) with a 0.1 °C step was used to regulate the T-Control Module's temperature between 18, 22, and 26 °C.

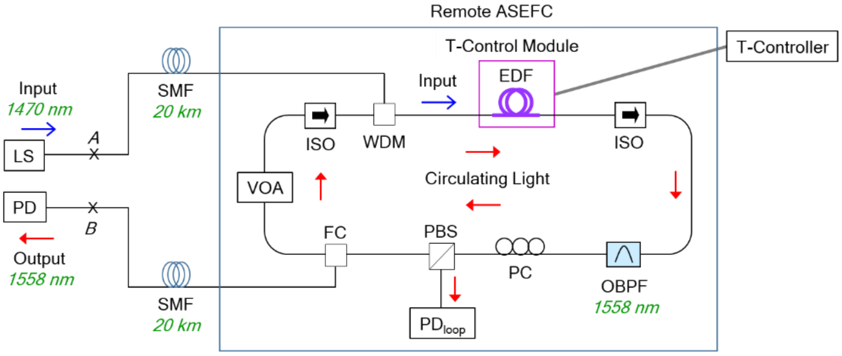

Fig. 2.20 Experimental configuration. (Copyright(C) 2021 IEICE, [41] Fig. 1).

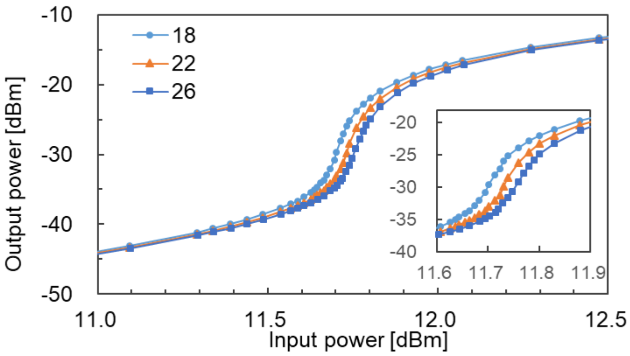

Fig. 2.21 Output power as a function of input power. (Copyright(C) 2021 IEICE, [41] Fig. 2).

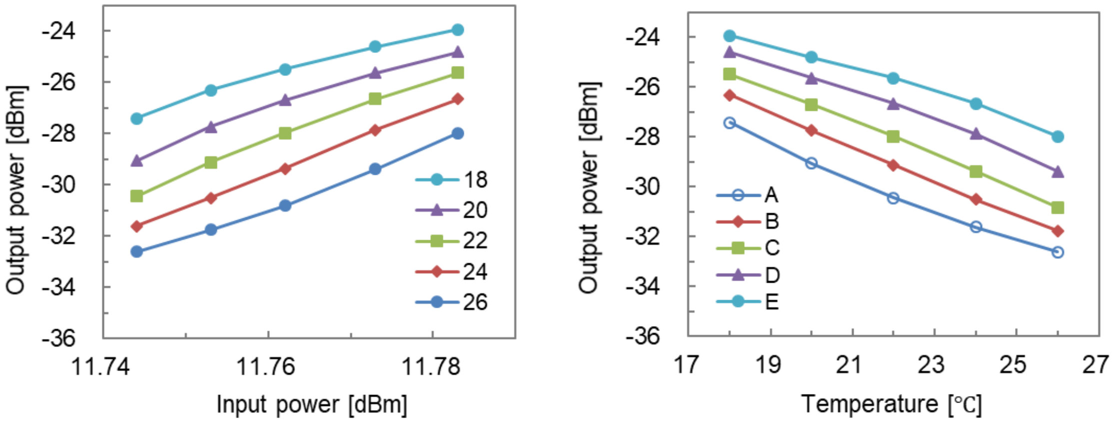

(a) (b)

Fig. 2.22 (a) Output power vs. input power at temperatures from 18 - 26 °C. (b) Output power vs. temperature. (Copyright(C) 2021 IEICE, [41] Fig. 3).

The relationship between the output power (P_{out}) and the input power (P_{in}) is depicted in Fig. 2.21. The values at Point-A and Point-B are P_{in} and P_{out}, respectively. The optical losses of the 20-km SMF are 4.1 and 3.9 dB, respectively, at 1470 and 1558 nm. The Fig. 2.21 in the picture are labeled 18, 22, and 26, respectively, representing the temperatures (T) at which the values of P_{out} are displayed. At T = 18, 22, and 26 °C, the input powers at the laser threshold are 11.688, 11.717, and 11.746 dBm, respectively. An essential portion of the curves surrounding the laser threshold may be magnified in the inset. Next, we define R_T as the ratio of the measuring system's power resolution (R_P) to its sensitivity's absolute value (S_{abs}): $R_T = R_P/S_{\mathrm{abs}}$. The assumption was to be R_P = 0.001 dB. P_{out} is shown as a function of P_{in} for T = 18, 20, 22, 24, and 26 °C in Fig. 2.22(a). The P_{in} ranges between 11.774 and 11.783 dBm. At P_{in} = 11.744, 11.753, 11.762, 11.773, and 11.783 dBm (known as as A, B, C, D, and E, respectively), Fig. 2.22(b) displays P_{out} as a function of T. Assuming R_P = 0.001 dB, Fig. 2.22(b) shows that at A, B, C, D, and E, respectively, S_{abs} = 0.649, 0.681, 0.668, 0.598, and 0.505 dB/°C and R_T = 0.00154, 0.00147, 0.00150, 0.00167, and 0.00198 °C. These values represent the averages for a range of 18 to 26 °C. Therefore, for P_{in} = 11.753 dBm, the maximum value of S_{abs} and the minimum value of

R_T are, 0.681 dB/°C and 0.00147 °C, respectively. The proposed fiber-optic measurement technique remote sensing method was successfully measure the temperature with a resolution of ~0.00147 °C in a remote distance of 20 km. The technique utilizes the temperature dependence of the gain of the EDF. Using the gain dependence of the ASEFC, the technique significantly improved the OPR and the sensitivity of the measurement scheme. In detail study discussed in Chapter-4 & 5.

3. ASEFC scheme for optical power sensing[1]

3.1. Background

One of the crucial components of fiber-optic measurement in optical communication and measurement systems using an optical power meter (PM) is the optical power resolution (OPR) [5, 6, 7, 8]. The PM is an electrically operated device which consists of a photodetector, such as a photodiode. The OPR of the PM is traditionally given in decibels (or percentages), and it is often on the order of 0.01 decibels (or 0.23%) [7, 8, 9, 10, 11]. For instance, a 0.01 dB OPR was published as a standard [8]. According to another illustration, the OPR is constrained by the PM's polarization dependency or interference noise phenomena, and the values for each of these phenomena range from ±0.005 to ±0.015 dB [7]. An innovative method was proposed for measuring optical power that considerably improved OPR by installing an amplified spontaneous-emission feedback circuit (ASEFC) upstream of a typical PM [18-23]. It was named as "ASEFC scheme." ASEFC operations occur near the lasing threshold region [9]. During this research, an optical loss measurement was demonstrated using a variable optical attenuator (VOA), with significant improvements in OPR of up to 67 times or more. The ASEFC technique achieved OPRs as low as 0.00014 dB (0.01/70 dB) or lower, where the display resolution for PM was 0.01 dB.

3.2. Experimental setup

The system configuration of the ASEFC scheme is shown in Fig. 3.1(a). A photodiode module (PDM) was utilized comprising an electric circuit and a photodiode. PDM is used numerous optical communication and sensing system applications. The ASEFC was

---

[1] This dissertation is based on “**Amplified-spontaneous emission feedback circuit scheme for optical measurement with improved optical power resolutions**” [27], by the same author, which appeared in the Proceedings of “IEICE Communication Express”, Copyright(C) 2022 IEICE.

[1] This dissertation is based on “Amplified-spontaneous emission feedback circuit scheme for optical measurement with improved optical power resolutions” [27], by the same author, which appeared in the Proceedings of “IEICE Communication Express”, Copyright(C) 2022 IEICE.

positioned in front of the PDM. The novel optical power meter proposed on the ASEFC system is called "ASEFC-PM", which consists of cascading ASEFC and PDM. The ASEFC-PM was used to calculate the optical power of the signal coming from a light source (LS). Between the LS and ASEFC, an optical device under test (DUT) was positioned. Though the DUT is an optical amplifier or a passive optical component, the DUT's gain and loss can measured, respectively. The light coming out of the ASEFC (λ_{out}) has a different wavelength than the input light (λ_{in}) coming in. The input and output lights for the ASEFC were denoted by P_{in} and P_{out} in dBm, respectively. When the ASEFC is removed from the ASEFC-PM, the PM is turned to just the PDM and act as a conventional PM. The term "conventional scheme" refers to the optical power measurement method employing the conventional PM.

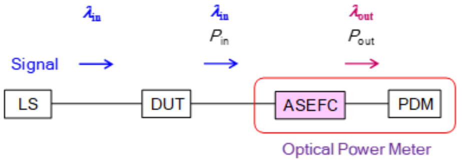

(a)

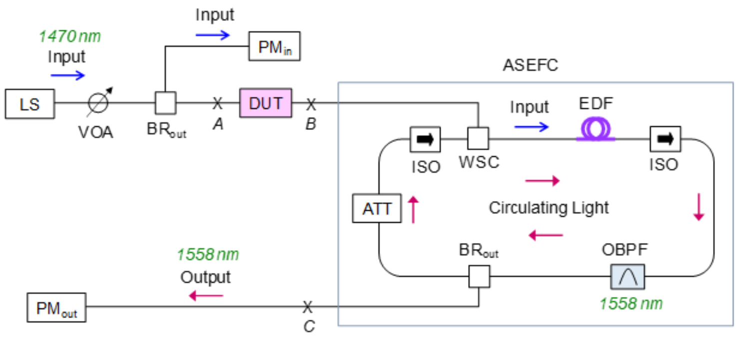

(b)

Fig. 3.1. (a) System configuration and (b) experimental setup of the ASEFC scheme. (Copyright(C) 2022 IEICE, [27] Fig. 1).

The experimental set-up, which included an LS, a DUT, an ASEFC, and a PM inserted after the ASEFC (PM$_{out}$), is shown in Fig. 3.1(b). After the LS, a VOA was set to change

---

[1] This dissertation is based on “Amplified-spontaneous emission feedback circuit scheme for optical measurement with improved optical power resolutions” [27], by the same author, which appeared in the Proceedings of “IEICE Communication Express”, Copyright(C) 2022 IEICE.

the P_{in}, designated as $\mathrm{VOA}_{\mathrm{LS}}$. Through a branch positioned after $\mathrm{VOA}_{\mathrm{LS}}$, $\mathrm{PM}_{\mathrm{out}}$ was used to measure P_{out} while $\mathrm{PM}_{\mathrm{in}}$ was used to monitor P_{in}. Each $\mathrm{PM}_{\mathrm{in}}$ and $\mathrm{PM}_{\mathrm{out}}$ sensor head was an Ando Electric AQ2735 with a polarization-dependent loss of 0.02 dB peak-to-peak or less. The sensor head's frequency bandwidth was set at around 20 Hz to lessen measurement noise, and the average number of times each measurement datum was averaged was set to 50. The LS included an InGaAsP type, Fabry-Perot laser diode (LD) with a constant drive current of 350 mA to maintain the output power and LD spectrum during the test. The measurement system had a warm-up time of at least two hours. While the minimal display resolution was 0.001 dB, the measured fluctuation in P_{in} with time was less than within approximately 0.001 and 0.005 dB peak-to-peak in the durations of about 5 and 60 minutes, respectively. The current and temperature of the driver for the LD were displayed with resolutions of 1 mA and 0.01 °C, respectively. The time variation of the current and temperature were estimated to be far less than the display resolutions.

The ASEFC has a fiber-ring feedback loop with a 15.9 m long erbium-doped fiber (EDF) spool as its gain medium. Around 1530 nm, the EDF's absorption peaked at about 4.7 dB/km. The ASEFC was composed of an optical bandpass filter (OBPF), two optical isolators (ISOs) on either side of the EDF, a wavelength-selective coupler (WSC), a branch for the output power ($\mathrm{BR}_{\mathrm{out}}$), and an attenuator (ATT) in the feedback loop. The input power range adjustment for the ASEFC, or lasing threshold adjustment, was performed using the ATT. In the C band, the EDF's average gain under the flat-gain spectrum condition was around 21 dB, while the loop loss of the feedback loop was about 15 dB. The OBPF's center wavelength and bandwidth were 1558 nm and 1 nm, respectively. With an increasing P_{in}, the gain of the EDF at 1558 nm approached 15 dB over the lasing threshold. λ_{in} is typically the gain medium's pump or signal wavelength

---

[1] This dissertation is based on “Amplified-spontaneous emission feedback circuit scheme for optical measurement with improved optical power resolutions” [27], by the same author, which appeared in the Proceedings of “IEICE Communication Express”, Copyright(C) 2022 IEICE.

[19, 23]. In this experiment, λ_{in} was selected to be a pump wavelength (1470 nm) of the EDF.

In Fig. 3.2(b) the optical powers, at points A, *B*, and *C* were denoted as P_{inDUT}, P_{in}, and P_{out} in dBm units, respectively. The DUT was a VOA (VOA_{DUT}), a product of Optoquest Co., Ltd. (Model VOAA), and it was made up of an optical interference section and a micrometer. The loss of the DUT (L_{DUT}), in dB units, is given by the following relation:

$$L_{\text{DUT}} = P_{\text{inDUT}} - P_{\text{in}}. \qquad (3.1)$$

At constant P_{inDUT}, the variation in L_{DUT} was denoted as ΔL_{DUT}. Subsequently, the following relation was obtained:

$$\Delta L_{\text{DUT}} = -\Delta P_{\text{in}}, \qquad (3.2)$$

Where ΔP_{in} was the difference in P_{in} caused by the loss variation of the DUT. Therefore, by using Eq. (3.2) we could derive $\Delta L_{\text{DUT.}}$ In Eq. (3.2) the measured values of ΔP_{in} was applied. In the conventional case, the ASEFC in Fig. 3.1(a) was removed so that the output power of VOA_{DUT} was measured by PM_{out} directly.

3.3. Experimental results and discussions

At the constant value of ΔL_{DUT}, Fig. 3.2(a) shows P_{in} as a function of P_{out}. The experimental data and a curve that was produced by numerical calculation are displayed in the figure. P_{in} changed from 15.729 to 15.887 dBm, or about 0.16 dB, while P_{out} changed from -28.212 to -17.502 dBm or about 10.7 dB. Here, a parameter was established, called "slope" or "sensitivity," which was the difference between P_{out} and P_{in}, represented by the symbol by $S \equiv \mathrm{d}P_{\text{out}}/\mathrm{d}P_{\text{in}}$. The sensitivity "$S$" coincided with an improvement factor in

---

[1] This dissertation is based on “Amplified-spontaneous emission feedback circuit scheme for optical measurement with improved optical power resolutions” [27], by the same author, which appeared in the Proceedings of “IEICE Communication Express”, Copyright(C) 2022 IEICE.

the OPR due to using the ASEFC system, if the excessive noise produced by the ASEFC was negligible.

To make the expressions of the equations in the following graph more straightforward, $x = P_{\mathrm{out}}$ and $y = P_{\mathrm{in}}$ were denoted. From Fig. 3.2(a), y is a function of x, that is, $y = f(x)$, and x is a function of y, that is, $x = g(y)$. The result is that g is an inverse function of f. the simple tangential function was used to explain the experimental data plot in Fig. 3.2(a):

$$y = b \cdot \tan\left(\frac{x-d}{ab}\right) + c, \tag{3.3}$$

Where a, b, c, and d are constants. Then, x and S (= $dP_{\mathrm{out}}/dP_{\mathrm{in}}$ = dx/dy) were given by

$$x = ab \cdot \arctan\left(\frac{y-c}{b}\right) + d, \tag{3.4}$$

$$S = \frac{ab^2}{b^2+(y-c)^2}, \tag{3.5}$$

Fig. 3.2(a) and (b) display the calculated values of the relationships provided by Eqs. (3.3) and (3.5), respectively. The values of the constants a, b, c, and d as 106, 0.047, 15.807, and 22.7, respectively, provided the best fit between the experimental and computed values in the range of Pout, from roughly 26.5 to 19.0 dBm where S was more than 60.

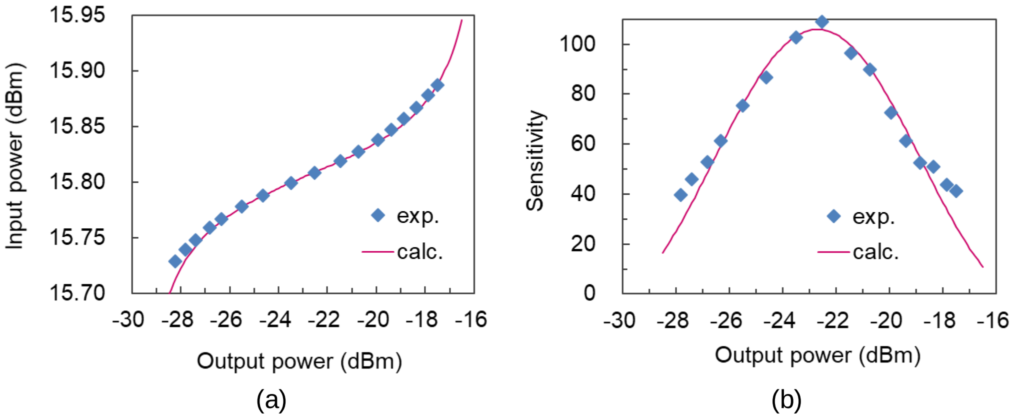

Fig. 3.2. (a) The input power and (b) the sensitivity as a function of the output power. Measured (exp.) and calculated (calc.) data are shown. (Copyright(C) 2022 IEICE, [27] Fig. 2).

---

[1] This dissertation is based on “Amplified-spontaneous emission feedback circuit scheme for optical measurement with improved optical power resolutions” [27], by the same author, which appeared in the Proceedings of “IEICE Communication Express”, Copyright(C) 2022 IEICE.

For the conventional method, we used $\mathrm{PM_{out}}$ to directly measure the output power from $\mathrm{VOA_{DUT}}$ (P_{outDUT}) as a function of the position of the micrometer $\mathrm{VOA_{DUT}}$ (z). P_{outDUT}(z) was used to represent P_{outDUT} at z. The display resolution of digital power meter $\mathrm{PM_{out}}$ (R_{PM}) was set to 0.001 dB, which was the lowest operating level possible. At constant P_{inDUT}, the loss of $\mathrm{VOA_{DUT}}$, that is, ΔL_{DUT}, was given by the relation $\Delta L_{\mathrm{DUT}}(z) = P_{\mathrm{outDUT}}(z=0) - P_{\mathrm{outDUT}}(z)$. ΔL_{DUT}(z) is depicted in Fig. 3.3(a) and (b) as a function of z in the plot regions for z = 0-1.4 mm in (a) and z = 0-1.0 mm in (b), respectively. The maximum value in this experiment for ΔL_{DUT} (z = 1.4 mm) was 0.015 dB, as shown in Fig. 3.3(a).

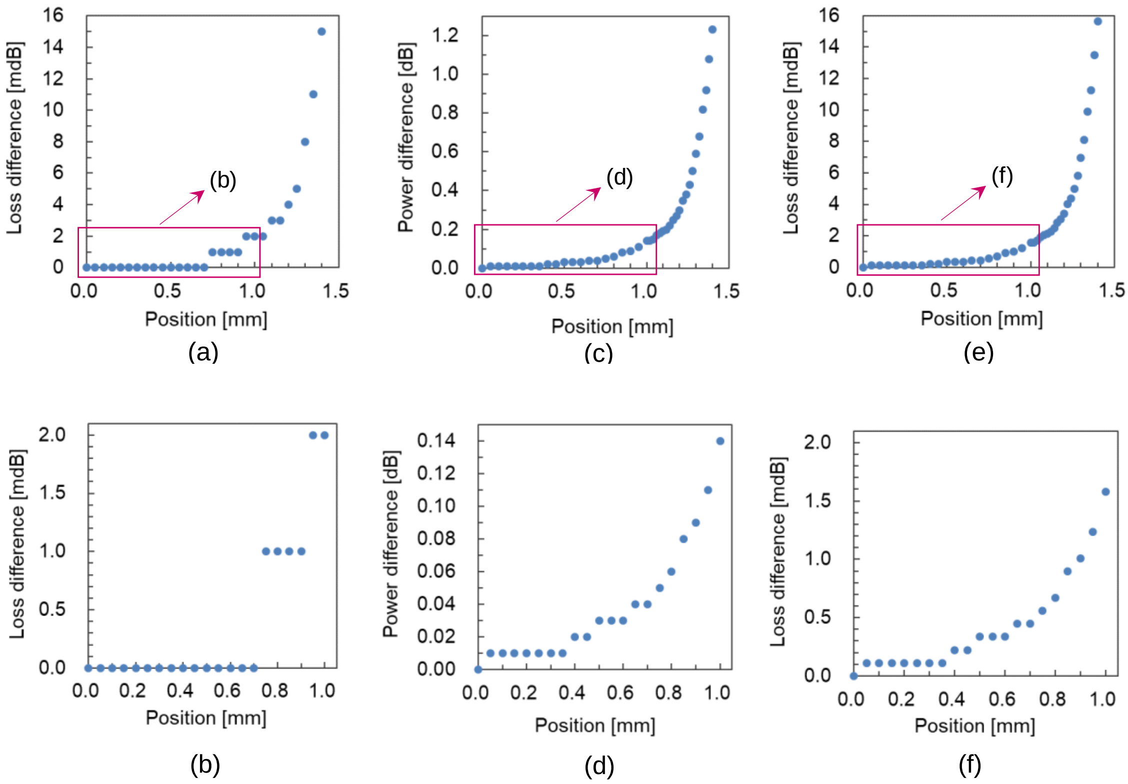

(a) (c) (e)

(b) (d) (f)

Fig. 3.3 **(a)** Measured losses of the $\mathrm{VOA_{DUT}}$ as a function of the micrometer position in the cases of the conventional scheme ((a) and (b)), and of the ASEFC scheme ((e) and (f)). The absolute values of the difference in optical power in the case of the ASEFC scheme are shown in (c) and (d). The regions of the micrometer position for the plots are 0-1.4 mm for (a), (c), and (e), and 0-1.0 mm for (b), (d), and (f). (Copyright(C) 2022 IEICE, [27] Fig. 3).

---

[1] This dissertation is based on “Amplified-spontaneous emission feedback circuit scheme for optical measurement with improved optical power resolutions” [27], by the same author, which appeared in the Proceedings of “IEICE Communication Express”, Copyright(C) 2022 IEICE.

For the ASEFC scheme, we measured P_{out} at z and used Eq. (3.3) to determine P_{in} at z. P_{out}(z) and P_{in}(z), were used to represent P_{out} and P_{in} at z, respectively. ΔP_{in} of Eq. (3.2) was given by $\Delta P_{\mathrm{in}}(z) = P_{\mathrm{in}}(z) - P_{\mathrm{in}}(z = 0)$. The difference in P_{out} was indicated as $\Delta P_{\mathrm{out}}(z) = P_{\mathrm{out}}(z) - P_{\mathrm{out}}(z = 0)$. In Fig. 3(c) and (d), the absolute values of ΔP_{out}(z) are displayed.

The absolute value of ΔP_{out} (z = 1.4 mm) in the ASEFC scheme (Fig. 3.3(c)) was 1.23 dB, which was 82 times greater than 0.015 dB. The excess noise in $P_{\mathrm{out}}(z)$ was determined to be less than several times 0.001 dB. The R_{PM} was then set in this ASEFC scheme scenario to 0.01 dB. The S had a maximum value of 15.807 dBm, which was 0.002 dB less than the input power at 15.787 dBm. $P_{\mathrm{in}}(z)$ was calculated using Eq. (3.4), so that $\Delta P_{\mathrm{in}}(z)$ was derived from the relation $\Delta P_{\mathrm{in}}(z) = P_{\mathrm{in}}(z) - P_{\mathrm{in}}(z = 0)$. Moreover, using Eqs. (3.2) and (3.5) the value of ΔL_{DUT} and S were derived, respectively. $\Delta L_{\mathrm{DUT}}(z)$ is shown as a function of z in Fig. 3.3(e) and (f). S as a function of z ($S(z)$), decreased with z from $S(z = 0$ mm$) = 89.8$, to $S(z = 1.4$ mm$) = 67.3$. The OPR at z ($R_{\mathrm{ASEFC}}(z)$) was presented by $R_{\mathrm{ASEFC}}(z) = R_{\mathrm{PM}} \,/\, S(z)$. Therefore, $R_{\mathrm{ASEFC}}(z)$ was 0.00011 dB (0.11 mdB) for the position of $z = 0$ mm, and 0.00014 dB (0.14 mdB) for the position of $z = 1.4$ mm. There was no random time variation or fluctuation in $P_{\mathrm{out}}(z)$ that is larger than 0.01 dB, as can be observed in the plots of Fig. 3.3(c) and (d). As a result, it was determined that in this measurement, the time variation in P_{inDUT} was less than within 0.00014 dB.

---

[1] This dissertation is based on “Amplified-spontaneous emission feedback circuit scheme for optical measurement with improved optical power resolutions” [27], by the same author, which appeared in the Proceedings of “IEICE Communication Express”, Copyright(C) 2022 IEICE.

3.4. Conclusion of the study

In order to achieve a significant improvement in OPR compared to the conventional measurement scheme, a novel method of optical power measurement was proposed and named "ASEFC". In addition, a simple analytical function expressing the relationship between P_{in} and Pout was proposed. As a result, the technique was successfully calculated P_{in} based on the value systematically measured for P_{out}. The OPR characteristics of the ASEFC scheme were demonstrated experimentally by measuring the loss variation of the VOA under test. The sensitivity/improvement factor was greater than 67, and the OPRs of the proposed ASEFC were less than 0.00014 dB when the display resolution of the power meter was 0.01 dB.

[1] This dissertation is based on “Amplified-spontaneous emission feedback circuit scheme for optical measurement with improved optical power resolutions” [27], by the same author, which appeared in the Proceedings of “IEICE Communication Express”, Copyright(C) 2022 IEICE.

4. Temperature-controlled ASEFC with improved OPR for optical sensing[2]

4.1 Background

High-resolution and stability is very essential for exceptionally sensitive, long-distance, wide-area, and reliable optical power measurements for fiber-optic sensing systems [1, 2, 3, 14]. The optical power resolution, or uncertainty is a crucial parameter of an optical power meter (PM). PM is often expressed in decibels (dB) or percentages (%). In a conventional scheme, it has an order of 0.01 dB (or 0.23%) [6-9]. Remarkably, the duration of the measurement has a significant impact on OPR. By utilizing an amplified-spontaneous-emission feedback circuit (ASEFC), a novel optical power measurement technique was proposed that may significantly increase the OPR compared to a standard PM [18-22]. In certain studies, the OPRs were increased using the ASEFC approach by improvement factors (IFs) ranging from 10 to 100. A gain medium, an erbium-doped fiber (EDF), or an optical semiconductor amplifier operating near the lasing threshold are all components of an ASEFC scheme [24].

In previous work, an optical variable attenuator's (VOA) loss variation was measured for a short period of time, less than around five minutes [22]. In this paper, a novel temperature-controlled ASEFC was proposed for long-term measurements in an experimental setup for remote fiber-optic sensing, and the accuracy and repeatability of the circuit were evaluated. It was observed that when the temperature of the ASEFC was not maintained during a lengthy experiment, accuracy and repeatability were considerably reduced [21]. The optical power emitted from the two different types of light sources was utilized in the setup. Therefore, the improved OPRs for one hour measurement was better (smaller) than 0.0001 dB or 0.10 mdB, where mdB stands for milli dB (10^{-3} dB).

---

[2] This dissertation is based on "**High-resolution and Stable optical power measurement using a temperature controlled amplified-spontaneous-emission feedback circuit**" [28], by the same author, which appeared in the Proceedings of "IEICE Communication Express", Copyright(C) 2023 IEICE.

[2] This dissertation is based on "High-resolution and Stable optical power measurement using a temperature controlled amplified-spontaneous-emission feedback circuit" [28], by the same author, which appeared in the Proceedings of "IEICE Communication Express", Copyright(C) 2023 IEICE.

4.2 Experimental configuration of ASEFC-based proposed measurement scheme

Fig. 4.1 depicts schematics of the (a) experimental setup and (b) configuration of ASEFC employed in this investigation. The experimental setup comprises of a light source (LS) and an ASEFC-based measurement system together, with a two-part measurement terminal and remote sensing section. A set of three single-mode fibers (SMFs) with a combined length of 20.0 km and an optical attenuator (ATT), simulating the test equipment, are included in the latter part. For instance, a sensor head for the measurand may take the role of ATT [1]. LS is either a fiber Bragg grating LD light source (FBG-LS) or a Fabry-Perot laser diode (LD) light source (FP-LS) with a polarization-multiplexed structure (Pol. MUX) [12, 13, 14]. For the ASEFC, LS emits pump light. The center power-averaged wavelengths for the FP-LS and FBG-LS, in particular, were 1472.0 and 1455.4 nm, respectively. For both LSs, variations in wavelength over a period of 30 minutes were as minor as 3 pm. For simplicity, the FBG-LS was only controlled by ACC whereas the FP-LS was driven by either the automated current control mode (ACC) or the automatic power control mode (APC) of its LD driver. While the minimum display resolutions for ACC and APC were 1 mA and 1 μA, the driving current for ACC and monitored photo-current for APC were 500 mA and 205 μA, respectively. Each LD was maintained at a constant temperature of 25.00 °C using an automated temperature management mode and a minimum display resolution of 0.01 °C. The pump light sent into an upstream SMF ($\mathrm{SMF_{up}}$) by the LS, FP-LS, or FBG-LS is shown in Fig. 4.1(a). Then, a fiber coupler (FC-1) launches 90% of its output into the ASEFC through the ATT, a VOA, a downstream SMF ($\mathrm{SMF_{down}}$), and a second FC (FC-2). Using the PM's sensor head ($\mathrm{PD_{in}}$), the pump power launched into the ASEFC was first measured. Then, a different sensor head ($\mathrm{PD_{out}}$) was used to measure the output power from the ASEFC. Ando Electric

---

[2] This dissertation is based on “High-resolution and Stable optical power measurement using a temperature controlled amplified-spontaneous-emission feedback circuit” [28], by the same author, which appeared in the Proceedings of “IEICE Communication Express”, Copyright(C) 2023 IEICE.

Co. (AQ2735) created each sensor head. For the ASEFC, the input and output powers are designated as P_{in} and P_{out} in dBm, respectively. By adjusting the loss of VOA, P_{in} was changed. The remaining 10% of the output light from FC-1 was instead directed into an optical spectrum analyzer (OSA) using an SMF for monitoring (SMF$_{\mathrm{moni}}$).

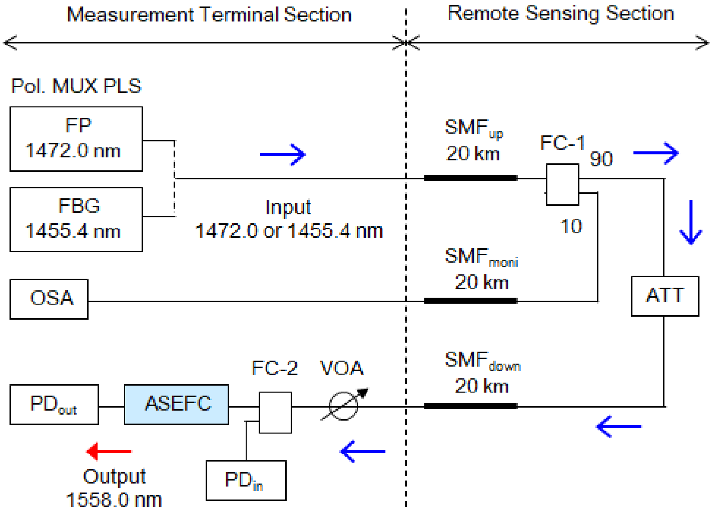

(a)

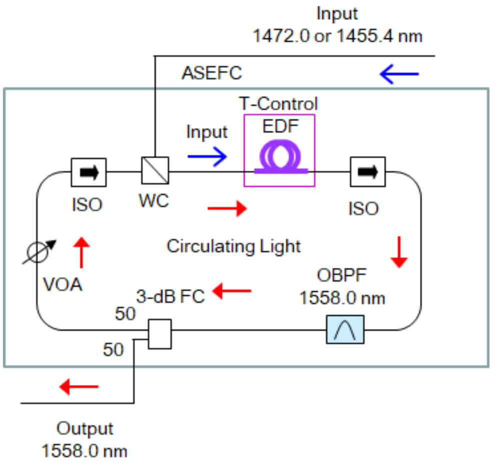

(b)

Fig. 4.1. Schematics of the (a) experimental setup and (b) ASEFC.
(Copyright(C) 2023 IEICE, [28] Fig. 1).

A temperature controller precisely maintained the temperature of the EDF's installation (called as T-Control) at 25.0 °C. The EDF had a 9.5 cm diameter and a spool length of 15.9 m. This is due to the fact that the ASEFC's P_{out} was heavily influenced by the surrounding temperature [10]. The temperature controller, model LDT 5416 from ILX Lightwave, has an hourly temperature stability of ±0.005 ℃ using a proportional/integral

---

[2] This dissertation is based on “High-resolution and Stable optical power measurement using a temperature controlled amplified-spontaneous-emission feedback circuit” [28], by the same author, which appeared in the Proceedings of “IEICE Communication Express”, Copyright(C) 2023 IEICE.

control strategy. Additionally, the EDF had a gain spectrum in the C band with a peak absorption of almost 100 dB near 1530 nm. The 3-dB transmission bandwidth for OBPF (λ_c) was 0.87 nm, and the center wavelength was set at 1558.0 nm. The total loss of the optical components in the fiber ring has been adjusted to approximately 15 dB at λ_c by modifying the loss of the VOA.

4.3 Experimental results and discussions

The improvement factor, IF is equal to the slope (S) of the curve of P_{out} versus P_{in}: $\mathrm{IF} = S \equiv \mathrm{d}P_{\mathrm{out}}/\mathrm{d}P_{\mathrm{in}}$ [18, 19, 20, 22]. The experimental outcomes employing the FP-LS ((a), (b), and (c)) and the FBG-LS ((d), (e), and (f)) are displayed in Fig. 4.2. The two types of LSs' pump light spectra are shown in Figs. 4.2(a) and (d). These results confirm the multi-longitudinal mode properties of the FP-LS and FBG-LS spectra, respectively shown in Figs. 4.2(a) and (d) [29, 30, 31]. Each spectrum is the result of the overlap of the two LD spectra that were utilized for polarization multiplexing. After polarization multiplexing, the 10-dB power reduction bandwidths of the FP-LS and FBG-LS are 10.3 nm and 1.5 nm, respectively, and there are 98 and 16 longitudinal modes in each of these devices.

P_{in} is depicted as a function of P_{out} in Figs. 4.2(b) and (e), while S is depicted as a function of P_{out} in Figs. 2(c) and (f). The average number was set to 50 and 200 for P_{in} and P_{out}, respectively, and the sample duration of the PM for both P_{in} and P_{out} was set to 20 ms. Four sets of plots, called M1, M2, M3, and M4, are illustrated using symbols in Figs. 4.2(b), (c), (e), and (f), and each inset displays a specific area of the plots. By computing the value of P_{in} from the measured value of P_{out}, a relation between P_{in} and P_{out} was discovered [6]. A fifth-order polynomial function of P_{out} can be used to represent P_{in}, and the following equation can be used to fit that function using the least-squares method:

$$y = \sum_{k=0}^{m} c_k\, x^k,\ x \equiv (P_{\mathrm{out}} - P_c), \qquad (4.1)$$

where y is the power of P_{in}, P_c is the center power at which the function S reaches its

---

[2] This dissertation is based on “High-resolution and Stable optical power measurement using a temperature controlled amplified-spontaneous-emission feedback circuit” [28], by the same author, which appeared in the Proceedings of “IEICE Communication Express”, Copyright(C) 2023 IEICE.

maximum value ($S_{\max}$), c_k are constants, and m is 5. For the sake of simplicity, only the example of M1 is shown in Figs. 4.2(b), (c), (e), and (f) with solid lines denoting the predicted P_{in} and S as a function of P_{out}. P_{c} were −24.70 and −24.14 dBm, and $S_{\max}$ were 107.3 and 102.8, for FP-LS and FBG-LS, respectively. The differences between the measured and calculated values of P_{in} ($P_{\text{in-m}}$ and $P_{\text{in-c}}$, respectively), $\delta P_{\text{in}} \equiv P_{\text{in}-\text{m}} - P_{\text{in}-\text{c}}$, were calculated for M1, and the resultant standard deviation of δP_{in} (σ) was calculated. σ for FP-LS and FBG-LS were 0.31 and 0.41 mdB, respectively. The uncertainty or OPR of the PM (ΔP_{PM}) in a short time of less than approximately 1 min ($\Delta P_{\text{PM-short}}$) and over a long time of more than approximately 1 min ($\Delta P_{\text{PM-long}}$) were estimated to be approximately 1 mdB and 10 mdB peak-to-peak, respectively. Based on measurements that integrate the above-mentioned experimental findings, this estimation was made.

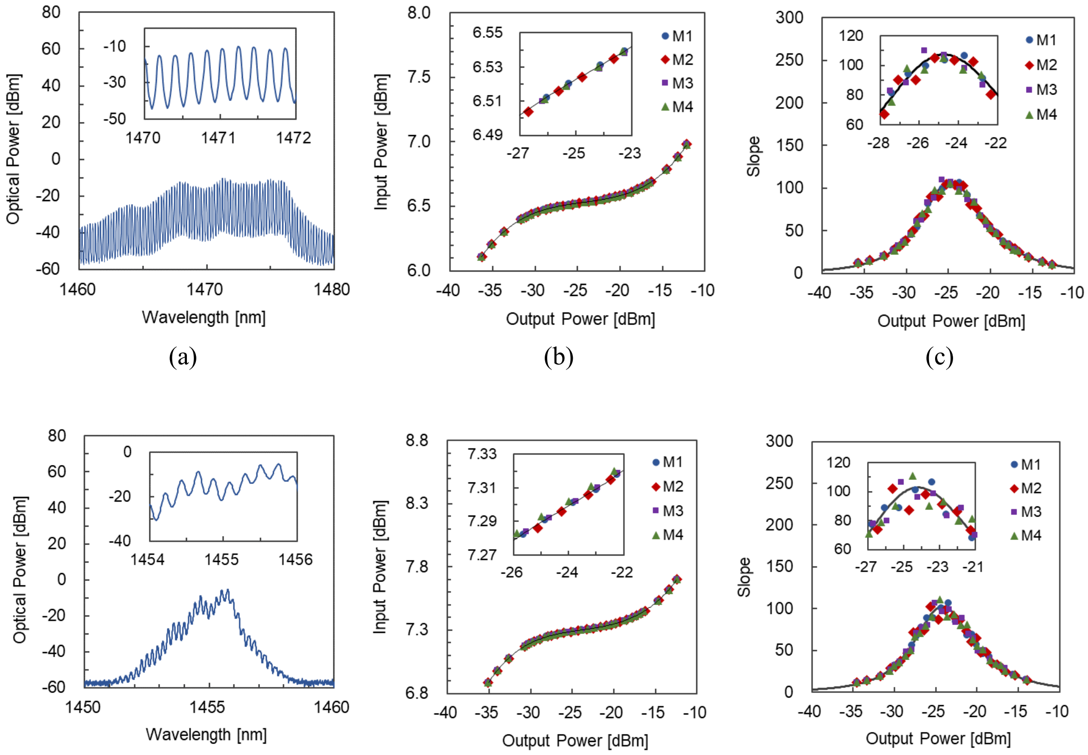

(a) (b) (c)

(d) (e) (f)

Fig. 4.2. Experimental results when using the FP-LS ((a), (b), and (c)) and the FBG-LS ((d), (e), and (f)). (a) and (d) Optical spectra of the pump lights. (b) and (e) The input power versus the output power. (c) and (f) The slope versus the output power. (Copyright(C) 2023 IEICE, [28] Fig. 2).

The time dependence of P_{in}, measured using the conventional technique (PD) and

---

[2] This dissertation is based on “High-resolution and Stable optical power measurement using a temperature controlled amplified-spontaneous-emission feedback circuit” [28], by the same author, which appeared in the Proceedings of “IEICE Communication Express”, Copyright(C) 2023 IEICE.

calculated using the proposed ASEFC technique (FC) is depicted in Fig. 4.3, whose powers are denoted as $P_{\text{in-m}}(t)$ and $P_{\text{in-c}}(t)$, respectively, where t is the time. The measured output power is denoted as $P_{\text{out-m}}(t)$. In particular, the figure includes the results for (a) FP-LS under APC, (b) FP-LS under ACC, and (c) FBG-LS under ACC. The values of $P_{\text{in-m}}(t)$ and $P_{\text{out-m}}(t)$ were read out with a minimum display resolution of 1 mdB of PM. $P_{\text{in-c}}(t)$ was calculated by substituting the data for $P_{\text{out-m}}(t)$ into the fitting function of Eq. (4.1) for FP-LS and FBG-LS. Fig. 4.3 shows the power differences in $P_{\text{in-m}}(t)$ and $P_{\text{in-c}}(t)$, defined as $\Delta P_{\text{m}}(t) \equiv P_{\text{in-m}}(t) - P_{\text{in-m}}(0)$ and $\Delta P_{\text{c}}(t) \equiv P_{\text{in-c}}(t) - P_{\text{in-c}}(0)$, respectively. As a typical example, each inset shows two sets of plots for the first five minutes. $P_{\text{out-m}}(0)$ in the cases of Figs. 4.3(a), (b), and (c) are −24.34, −24.40, and −24.10 dBm, respectively. The minimum S (S_{min}) calculated for the data in Fig. 4.3 are 106.0, 105.2, and 96.7, respectively.

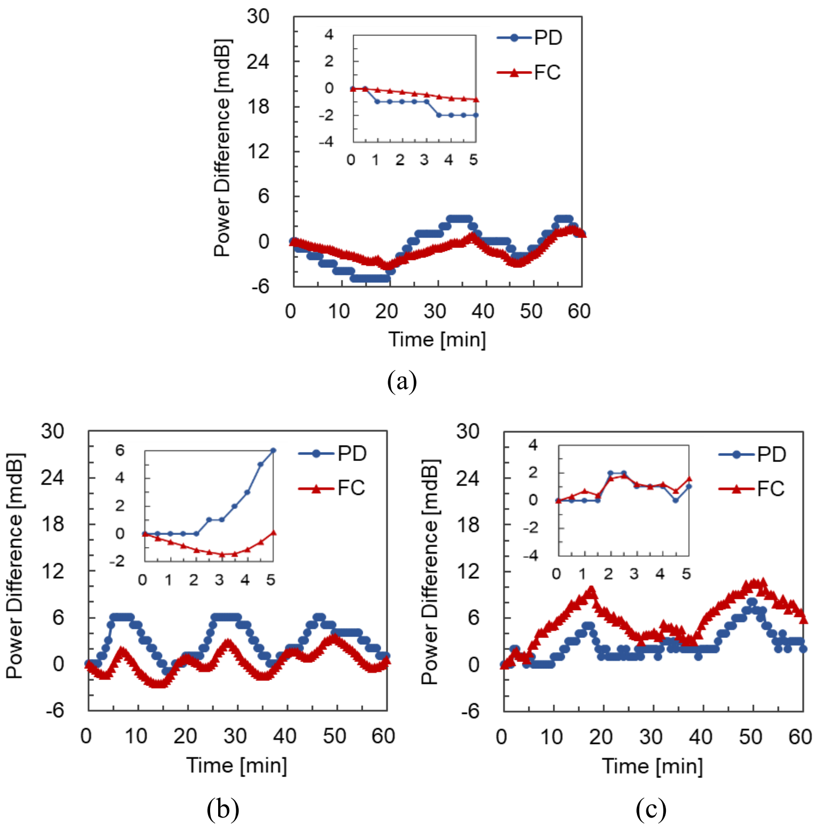

(a)

(b)

(c)

Fig. 4.3. Characteristics of the time dependence of the input pump power measured by the conventional technique (PD) and calculated by our proposed ASEFC technique (FC) for (a) the FP-LS under APC, (b) the FP-LS under ACC, and (c) the FBG-LS under ACC. (Copyright(C) 2023 IEICE, [28] Fig. 3).

---

[2] This dissertation is based on “High-resolution and Stable optical power measurement using a temperature controlled amplified-spontaneous-emission feedback circuit” [28], by the same author, which appeared in the Proceedings of “IEICE Communication Express”, Copyright(C) 2023 IEICE.

Therefore, the maximum OPR ($\Delta P_{\text{ASEFC-max}} = \Delta P_{\text{PM}}/S_{\text{min}}$) are 0.094, 0.095, and 0.10 mdB, for Figs. 4.3(a), (b), and (c), respectively, when an uncertainty $\Delta P_{\text{PM-long}}$ of 10 mdB for ΔP_{PM} was considered. The OPRs in the three cases of Figs. 4.3(a), (b), and (c) are better (smaller) than the largest value of the $\Delta P_{\text{ASEFC-max}}$ of 0.10 mdB when the IF (S_{min}) of approximately 97 was used. The length of the time variations in $\Delta P_{\text{c}}(t)$ in Figs. 4.3(a), (b), and (c) are 4.8, 6.0, and 10.7 mdB, respectively. The difference in absolute terms between $\Delta P_{\text{m}}(t)$ and $\Delta P_{\text{c}}(t)$ is defined as $\Delta P \equiv |\Delta P_{\text{m}}(t) - \Delta P_{\text{c}}(t)|$. The average and maximum of ΔP for the three measurements of Figs. 4.3(a), (b), and (c) were 2.5 and 5.0 mdB, respectively. As shown in Fig. 4.3, the value of $\Delta P_{\text{m}}(t)$ and $\Delta P_{\text{c}}(t)$ coincide within an inaccuracy of $\Delta P_{\text{m}}(t)$, which is $\Delta P_{\text{PM-long}}$ of ± 5 mdB (10 mdB, peak to peak). The small variations in ambient temperature near the LD modules of the FP-LS and FBG-LS, as well as the APC and ACC operations, may be the causes of the time fluctuations of $\Delta P_{\text{c}}(t)$.

---

[2] This dissertation is based on “High-resolution and Stable optical power measurement using a temperature controlled amplified-spontaneous-emission feedback circuit” [28], by the same author, which appeared in the Proceedings of “IEICE Communication Express”, Copyright(C) 2023 IEICE.

4.4 Conclusion of the study

The proposed technique for optical power measurement uses an ASEFC that can be temperature controlled, with several improvements such as high resolution and better stability. Improvement factors more significant than 97 evaluated both the OPR and stability aspects of the method. The P_{in} was determined by applying a fifth-order polynomial function starting with P_{out}. Results showed that P_{in} could be determined with high levels of accuracy and repeatability using this calculation. The optical power of the lights emitted from the FP-LS and FBG-LS were precisely measured, with small time variations up to 10.7 mdB. Assuming that $\Delta P_{\mathrm{PM\text{-}long}}$ for one hour was equal to 10 mdB, the OPR was found to be better than 0.10 mdB ($\Delta P_{\mathrm{ASEFC\text{-}max}}$). Detailed analysis and minimization of the time fluctuations are expected to pose new challenges in the future.

---

[2] This dissertation is based on “High-resolution and Stable optical power measurement using a temperature controlled amplified-spontaneous-emission feedback circuit” [28], by the same author, which appeared in the Proceedings of “IEICE Communication Express”, Copyright(C) 2023 IEICE.

5. Bandwidth and dynamic range characteristics of ASEFC[3]

5.1 Background

For many optical measurement system applications, including long-distance and wide-area sensing, loss measurements of optical devices and components in optical communication systems, and industrial and environmental sensing, fiber-optic sensing is a crucial and indispensable technology [1, 2, 3, 4]. Fiber-optic sensing is particularly useful for sensing over long distances and large areas. Optical power meters are among the most fundamental instruments typically utilized in optical measuring systems. Particularly because of their exceptional performance in the areas of low noise, excellent stability, and high optical power resolution (OPR), power meters (PM) based on photodiodes (PD) are frequently used. The OPR of the PM, which is also known as uncertainty, is usually represented in decibels (or percentages), and its values are restricted to being on the order of 0.01 decibels (or 0.23%) [11, 12, 13, 14]. Most of the OPR in typical modern PMs is thought to result from interference noise and polarization dependency.

We have recently developed a novel optical power measurement method that significantly improved the OPR compared to that of the state-of-the-art PMs by employing an amplified-spontaneous-emission (ASE) feedback circuit (ASEFC) placed in front of a PM [18-23]. This method is referred to as the "ASEFC technique." The erbium-doped fiber (EDF) or optical semiconductor amplifier (SOA), a gain medium, and a feedback fiber loop establish the ASEFC. Furthermore, it operates relatively close to the lasing threshold [23, 24, 25]. Due to the laser generally operating in a region significantly above the lasing threshold, the ASEFC differs from the laser in this regard. Furthermore, in the

---

[3] This dissertation is based on “**Amplified-spontaneous-emission feedback circuit with wide operating bandwidth and dynamic range**” [54], by the same author, which appeared in the Proceedings of “IEICE Electronics Express”, Copyright(C) 2023 IEICE.

[3] This dissertation is based on “Amplified-spontaneous-emission feedback circuit with wide operating bandwidth and dynamic range” [54], by the same author, which appeared in the Proceedings of “IEICE Electronics Express”, Copyright(C) 2023 IEICE.

case of the ASEFC, the wavelength of the output light differs from that of the input light. This works fundamentally differs from an optical amplifier where the two wavelengths coincide. By employing the nonlinear relationship within the input and output powers measured in dBm, the ASEFC technique improved the OPR by factors (improvement factors) of the order of 10-100 [18, 19, 21, 22].

In particular, a variable optical attenuator (VOA)'s small loss variation was measured in an earlier study with an enhanced OPR of 0.14 mdB, where mdB stands for milli dB (10^{-3} dB) [32]. In a different investigation, the fluctuations in the optical power were measured using two kinds of pump light sources frequently utilized in optical transmission systems [33]. Pump lights with wavelengths of 1472 or 1455 nm were employed in both trials as the ASEFC input light for the EDF [35]. Therefore this kind of circuit was referred to as "ASEFC-P." A subsequent study provided experimental proof of the viability of 20 km long fiber-optic remote sensing.

In this study, a novel ASEFC was proposed that operates using an input light with signal wavelengths of EDF. The wavelength region is up to 30 nm, from 1530 to 1560 nm. This type of circuit is called “ASEFC-S.” Experimental research examined the ASEFC-S's wide operational bandwidth and dynamic range properties. Due to the large dynamic range properties of the proposed ASEFC-S, it could also effectively demonstrate fiber-optic remote sensing across a distance of 50 km.

5.2 Experimental setup

The experimental setup is depicted in a schematic form in Fig. 5.1. Figure 5.1(a), (b), and (c) show the configurations of the measurement system, an ASEFC, and an ASE light source (ASELS), respectively. Both a remote sensing section (RSS) and a measurement terminal section (MTS) were components of the measuring system. The device put to the test (VOA_{DUT}) was an ASELS with an average wavelength of 1559.3 nm that was used in

---

[3] This dissertation is based on “Amplified-spontaneous-emission feedback circuit with wide operating bandwidth and dynamic range” [54], by the same author, which appeared in the Proceedings of “IEICE Electronics Express”, Copyright(C) 2023 IEICE.

the MTS for remote sensing the loss of a VOA. In some other systems, the VOA$_{\mathrm{DUT}}$ can be substituted for a sensor head [1, 2, 3, 4]. The VOA$_{\mathrm{DUT}}$ used in this study, Model VOAA from Optoquest Co., Ltd., consists of an optical beam alignment part and a micrometer. The ASEFC, which is placed on the light detection side, also uses the laser light produced by a tunable light source (TLS) as its input light. The TLS has been adjusted to operate in the wavelength range of 1530 and 1560 nm. In the case when the RSS was not utilized, the ASELS or TLS may be switched on and off at locations A and B by splicing together the optical connectors.

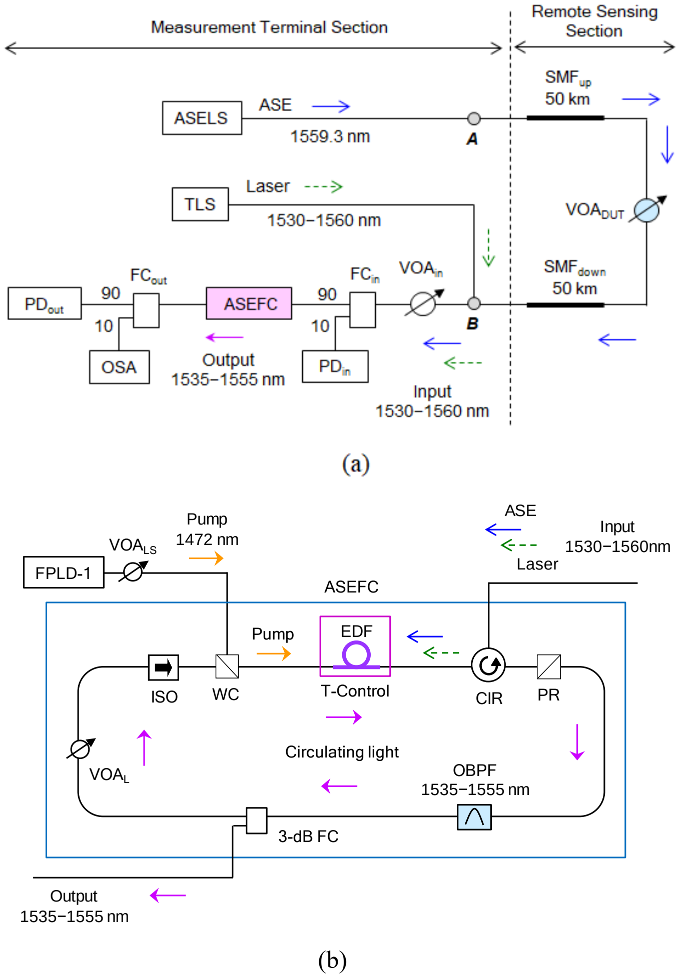

Fig. 5.1 Schematic experimental setup. Configurations of the (a) measurement system, (b) ASEFC, (Copyright(C) 2023 IEICE, [54] Fig. 1).

The light from the ASELS or TLS was launched into the ASEFC on the input portion of the device using a VOA (VOA$_{\mathrm{in}}$) and fiber coupler (FC$_{\mathrm{in}}$). The “λ_{in}" stands for the input

---

[3] This dissertation is based on “Amplified-spontaneous-emission feedback circuit with wide operating bandwidth and dynamic range” [54], by the same author, which appeared in the Proceedings of “IEICE Electronics Express”, Copyright(C) 2023 IEICE.

light's average wavelength. The branching ratios for the FC_{in} were 90%:10%. A PD module or PM (PD_{in}) that was connected to the 10% port of FC_{in} was used to monitor the power of input light (P_{in} in dBm). An optical spectrum analyzer (OSA) and another fiber coupler (FC_{out}) were used to measure the light that the ASEFC emits. PD_{out} connected to FC_{out}'s 90% port was used to monitor the power of output light (P_{out} in dBm). Both PD_{in} and PD_{out} were the same type of optical sensor head (Ando Electric Co. (AQ2735)). The optical sensor head used by PD_{in} and PD_{out} (made by Ando Electric Co., model number AQ2735) was the same. The output light (λ_{out}) had an average wavelength in the range of 1535 to 1555 nm. The RSS also included VOA_{DUT} and two 50 km single-mode fibers (SMFs, G.652), one for upstream flow (SMF_{up}), and the other for downstream flow (SMF_{down}).

The Fig. 5.1(b) is configuration of the ASEFC. The ASEFC consists of an EDF as a gain medium and a feedback fiber loop. The loop comprises several fiber modules, which are a tunable optical bandpass filter (OBPF), a 3-dB fiber coupler (FC), a VOA (VOA_L), an optical isolator (ISO), a wavelength-selective coupler (WC), an optical circulator (CIR), and a pump rejection filter (PR). The pump light for the EDF was emitted by a Fabry-Perot type laser diode module (FPLD-1), and the pump power launched into the ASEFC (P_p) and then the EDF was changed by setting a VOA (VOA_{LS}) following the FPLD-1. FPLD-1 had an average wavelength of 1472 nm. The temperature control module (T-Control) that maintained the EDF was kept at a constant temperature of 23.0 °C by employing a temperature controller. The EDF was a 15.9 m spool with a diameter of 9.5 cm. The PR rejected the EDF's residual pump light after it had passed through the CIR. Additionally, the 3-dB transmission bandwidth was set to be approximately 0.87 nm, and the center wavelength of the OBPF (λ_c) was set to 1535–1565 nm. By adjusting the loss of VOA_L, the overall optical loss of the loop was changed. Additionally, a portion of the circulating light was branched by the 3-dB FC to emit the output light of ASEFC where

---

[3] This dissertation is based on "Amplified-spontaneous-emission feedback circuit with wide operating bandwidth and dynamic range" [54], by the same author, which appeared in the Proceedings of "IEICE Electronics Express", Copyright(C) 2023 IEICE.

λ_{out} coincided with λ_{c}.

The light wavelengths from the ASELS and TLS coincided with the EDF signal wavelengths in the C-band. The ASEFC operates close to the fiber loop's lasing threshold, which contains EDF. With increasing input power of the signal light, the population probability of the upper laser level ($^4\mathrm{I}_{13/2}$) of the EDF (N_2) decreased. In contrast, N_2 increased in our earlier studies with the input power of the pump light with wavelengths of 1472 or 1455 nm [18, 20, 21, 22, 23].

5.3 Experimental results and discussions

5.3.1 Wideband characteristics of ASEFC

P_{in} is displayed as a function of P_{out} in Fig. 5.2(a) at in values of 1530, 1540, 1550, and 1560 nm. The measured values (labeled "m") and calculated values (labeled "c") are plotted in the figure, respectively, using symbols and lines. For P_{in} and P_{out}, the average numbers were set to 50 and 200, respectively, and the sampling time of the PM for both was set to 20 ms. Additionally, λ_{c} was chosen to be either a longer or shorter value by separating it by 5 nm from λ_{in}, so that for 1530, 1540, 1550, and 1560 nm, λ_{c} was 1535, 1535, 1545, and 1555 nm, respectively.

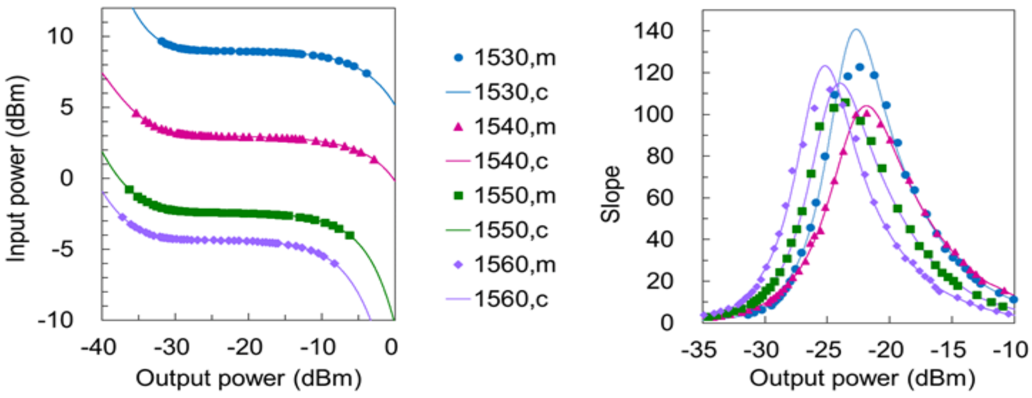

(a) (b)

Fig. 5.2 (a) Input powers and (b) slopes as a function of the output power at the input wavelengths of 1530, 1540, 1550, and 1560 nm. Symbols and lines show measured and calculated values, respectively**.** (Copyright(C) 2023 IEICE, [54] Fig. 2).

---

[3] This dissertation is based on “Amplified-spontaneous-emission feedback circuit with wide operating bandwidth and dynamic range” [54], by the same author, which appeared in the Proceedings of “IEICE Electronics Express”, Copyright(C) 2023 IEICE.

From the data presented in Fig. 5.2(a), the slopes were calculated from each curve (S), which are defined as the differential coefficients of P_{out} against P_{in}:

$$S \equiv -\mathrm{d}P_{\mathrm{out}}/\mathrm{d}P_{\mathrm{in}}. \qquad (5.1)$$

In contrast to the ASEFC-P, this ASEFC-S has a quantity $\mathrm{d}P_{\mathrm{out}}/\mathrm{d}P_{\mathrm{in}}$ with the opposite sign. S might contribute to the OPR's improvement [18, 20, 21, 22, 23]. At λ_{in} = 1530, 1540, 1550, and 1560 nm, S is depicted in Fig. 5.2(b) as a function of P_{out} in a manner similar to that in Fig. 5.2(a). We used the fitting functions derived from the measured data of P_{in} and P_{out} in the proposed ASEFC technique to calculate P_{in} from the measured P_{out}. The algebraic functions in equation are of fifth order.

$$P_{\mathrm{in}} = \sum_{k=0}^{5} c_k \, P_{\mathrm{out}}^{k}, \qquad (5.2)$$

where c_k is a constant [22]. It was discovered that as P_{p} increased and the loss of VOA$_{\mathrm{L}}$ (L_{loop}) decreased, the maximum slope (S_{max}) increased. As a result, S_{max} can be set to any value. As seen in Fig. 5.2(b), S_{max} was set to be higher than or equal to 100. There are two different types of S, the measured or calculated data (S_{m} or S_{c}) and they are both calculated using the equation below:

$$S_{\mathrm{a}} = \Delta P_{\mathrm{out}}/\Delta P_{\mathrm{in}}, \qquad (5.3)$$

where a = m or c and ΔP_{in} and ΔP_{out} are the incremental values of P_{in} and P_{out}, respectively. For S_{m}, ΔP_{in} has been set to roughly 0.01 dB, whereas for S_{c}, ΔP_{out} had been established to 0.01 dB. The S_{m} values were less than the S_{c} values close to the areas with the highest slopes, as seen in Fig. 5.2(b). This is due to the fact that while ΔP_{out} for S_{c} is precisely small, ΔP_{in} for S_{m} is not small enough. For λ_{in} at 1530, 1540, 1550, and 1560 nm, the corresponding P_{p} values were 40.8, 42.8, 18.2, and 11.8 mW. Additionally, the S_{c} values were 141, 104, 115, and 123, for λ_{in} at 1530, 1540, 1550, and 1560 nm, respectively.

[3] This dissertation is based on “Amplified-spontaneous-emission feedback circuit with wide operating bandwidth and dynamic range” [54], by the same author, which appeared in the Proceedings of “IEICE Electronics Express”, Copyright(C) 2023 IEICE.

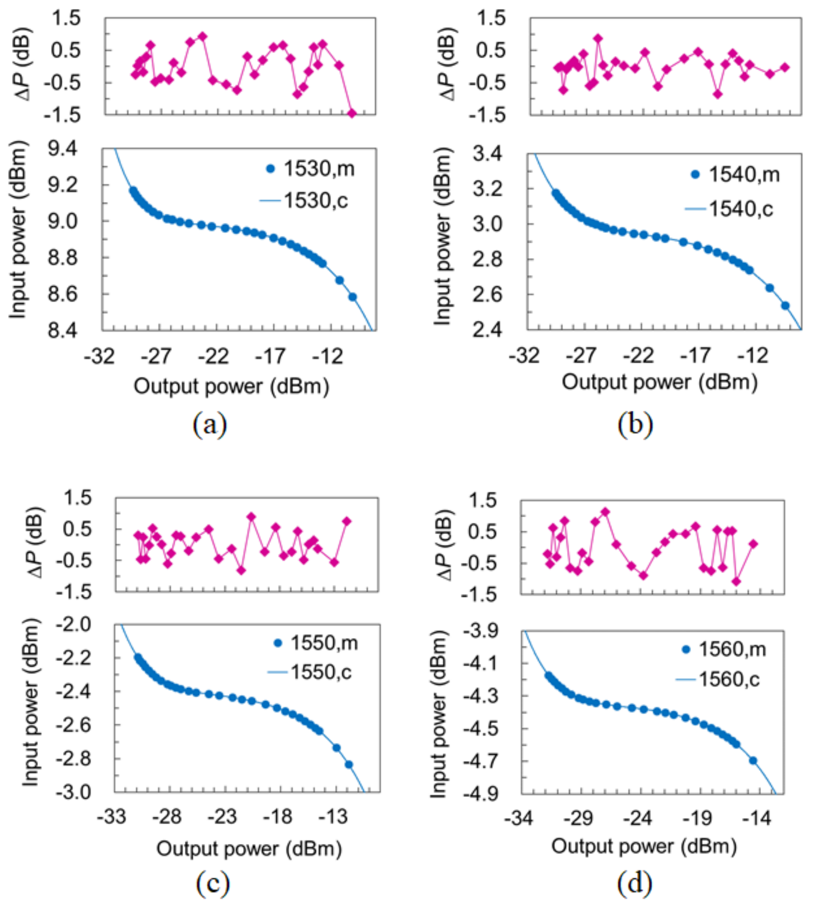

(a) (b)

(c) (d)

Fig. 5.3 Input power and power difference (ΔP) as a function of the output power for the input signal wavelengths of (a) 1530, (b) 1540, (c) 1550, and (d) 1560 nm. (Copyright(C) 2023 IEICE, [54] Fig. 3).

At maximum slope conditions, the values of input power and output power are denoted as $P_{\text{in-0}}$ and $P_{\text{out-0}}$, respectively. The fitting functions described in Eq. (5.2) were used to calculate the values of $P_{\text{in-0}}$ and $P_{\text{out-0}}$ for input power and output power, respectively. For λ_{in} values of 1530, 1540, 1550, and 1560 nm, the value of $P_{\text{in-0}}$ ranged from 8.98 dBm to -4.37 dBm, while the value of $P_{\text{out-0}}$ ranged from -22.68 dBm to -25.18 dBm. Therefore, $P_{\text{in-0}}$ decreases with increasing λ_{in} and achieves a minimum value of -4.37 dBm among the four investigated λ_{in} wavelengths. Figure 5.3 depicts detailed plots of the data presented in Fig. 5.2(a). Specifically, the measured data of input power (P_{in}) for S (S_{m} and S_{c}) values greater than 10 are displayed as a function of output power (P_{out}). The calculated curves are also displayed in the figure. The plots for λ_{in} at 1530, 1540, 1550, and 1560 nm are illustrated in Figures 5.3(a), (b), (c), and (d), respectively. Moreover, we computed the

[3] This dissertation is based on “Amplified-spontaneous-emission feedback circuit with wide operating bandwidth and dynamic range” [54], by the same author, which appeared in the Proceedings of “IEICE Electronics Express”, Copyright(C) 2023 IEICE.

difference (ΔP) between the measured and calculated input powers ($P_{\text{in-m}}$ and $P_{\text{in-c}}$): The difference (ΔP) is defined as $\Delta P \equiv P_{\text{in}-\text{m}} - P_{\text{in}-\text{c}}$. We depict how ΔP varies with respect to P_{out} and display it on Figure 5.3. The distributions of the ΔP against the output power (P_{out}) showed some random characteristics. The standard deviations of ΔP (σ) were calculated as 0.55, 0.38, 0.43, and 0.61 mdB for the input wavelengths (λ_{in}) of 1530, 1540, 1550, and 1560 nm, respectively.

5.3.2 Dynamic range characteristics of the ASEFC

The input-output characteristics of the ASEFC were studied by using the ASELS in place of the TLS. The ASELS wavelength (1559.3 nm) was selected as it produced the lowest P_{in} among the four wavelengths tested in Sec. 5.3.1 (Figs. 5.2 and 5.3) with a wavelength close to λ_{in} of 1560 nm. Figs. 5.4(a) and (b) illustrate the relationship between P_{in} and S concerning P_{out}, similar to Figs. 5.2(a) and (b). The value of λ_{c} was set to 1542.0 nm based on the ASELS output light's bandwidth characteristics shown in Fig. 5.6(a). Four conditions, namely A, B, C, and D, were achieved with varying values of S_{max} through proper selection of L_{loop} and P_{p}. For the respective conditions A, B, C, and D, the sets of values (S_{max}, L_{loop}, P_{p}) were as follows: (44, 7.7 dB, 7.6 mW), (74, 6.5 dB, 10.0 mW), (114, 4.7 dB, 15.2 mW), and (158, 3.0 dB, 22.4 mW). The values of S_{max} in each case were the result of the calculation. In addition, the corresponding sets of values ($P_{\text{in-0}}$, $P_{\text{out-0}}$), in dBm, for conditions A, B, C, and D were (-14.94, -26.67), (-11.28, -25.43), (-7.76, -24.64), and (-5.25, -23.86), respectively. Both $P_{\text{in-0}}$ and $P_{\text{out-0}}$ increase as S_{max} increases.

---

[3] This dissertation is based on “Amplified-spontaneous-emission feedback circuit with wide operating bandwidth and dynamic range” [54], by the same author, which appeared in the Proceedings of “IEICE Electronics Express”, Copyright(C) 2023 IEICE.

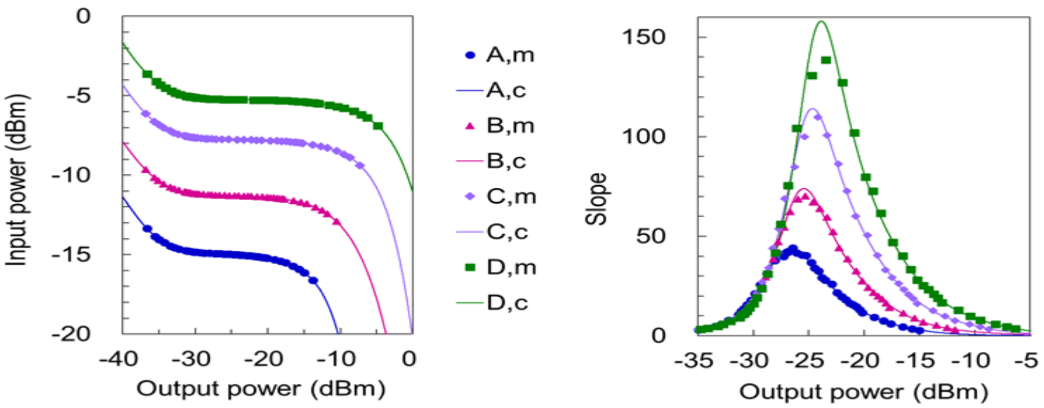

(a) (b)

Fig. 5.4 (a) Input power and (b) slope as a function of the output power at the operating conditions of A, B, C, and D. (Copyright(C) 2023 IEICE, [54] Fig. 4).

Fig. 5.5 displays an in-depth presentation of the data illustrated in Fig. 5.4(a), just like in Fig. 5.3. Figs. 5.5(a), (b), (c), and (d) display a set of plots of P_{in} and ΔP for the conditions of A, B, C, and D, respectively. For the conditions of A, B, C, and D, the σ values were 0.46, 0.47, 0.38, and 0.46 mdB, respectively. According to [6, 7, 22], it is postulated that significant portions of the value of ΔP arise because of interference noises in the measurement system and the time variation of P_{p} for both cases of Figs. 3 and 5.

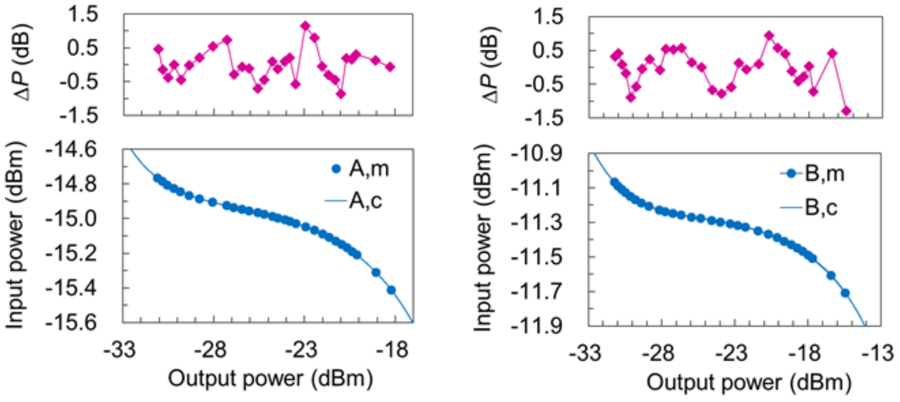

(a) (b)

---

[3] This dissertation is based on “Amplified-spontaneous-emission feedback circuit with wide operating bandwidth and dynamic range” [54], by the same author, which appeared in the Proceedings of “IEICE Electronics Express”, Copyright(C) 2023 IEICE.

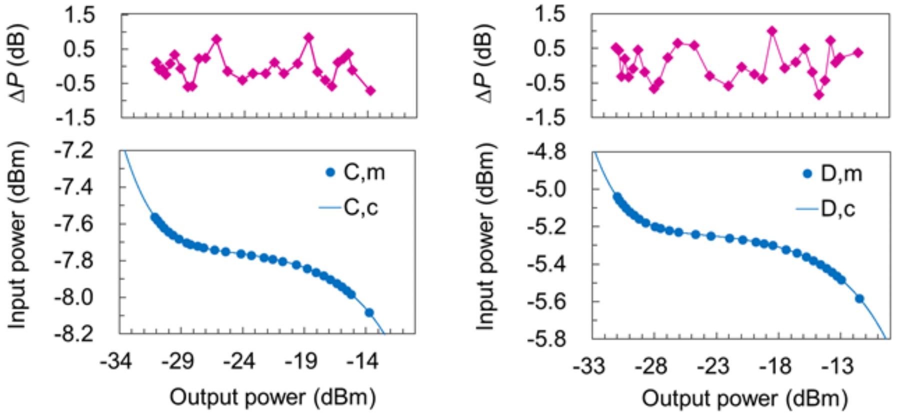

(c) (d)

Fig. 5.5 Input power and the power difference (ΔP) as a function of the output power at the operating conditions of (a) A, (b) B, (c) C, and (d) D**.** (Copyright(C) 2023 IEICE, [54] Fig. 5).

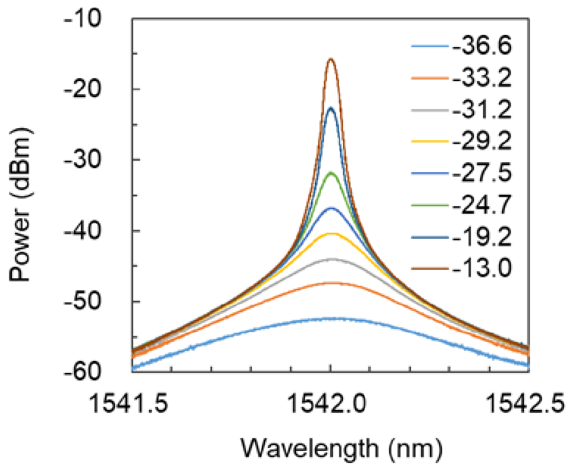

Fig. 5.6 output power spectra of the ASEFC at eight output powers**.** (Copyright(C) 2023 IEICE, [54] Fig. 6).

Figure 5.6 demonstrates the output power spectra of the ASEFC at a typical range of eight values for the parameter P_{out}. The OSA was calibrated to have a resolution of 0.03 nm (30 pm) for each wavelength. The eight sets of data (P_{out} in dBm, $\Delta\lambda_{3\text{dB}}$ in pm) from the top to bottom in Fig. 6(b) were (−36.6, 530), (−33.2, 363), (−31.2, 254), (−29.2, 163), (−27.5, 102), (−24.7, 59), (−19.2, 35), and (−13.0, 33). Fig. 5.7 shows the measured bandwidth $\Delta\lambda_{3\text{dB}}$ and calibrated bandwidth $\Delta\lambda_{3\text{dB-cal}}$ ($\equiv \Delta\lambda_{3\text{dB}} - \Delta\lambda_{\text{OSA}}$) as a function of P_{out}. It can be seen that $\Delta\lambda_{3\text{dB}}$ and $\Delta\lambda_{3\text{dB-cal}}$ decrease with P_{out} toward the maximum slope

[3] This dissertation is based on “Amplified-spontaneous-emission feedback circuit with wide operating bandwidth and dynamic range” [54], by the same author, which appeared in the Proceedings of “IEICE Electronics Express”, Copyright(C) 2023 IEICE.

operating point at P_{out} of −25 dBm.

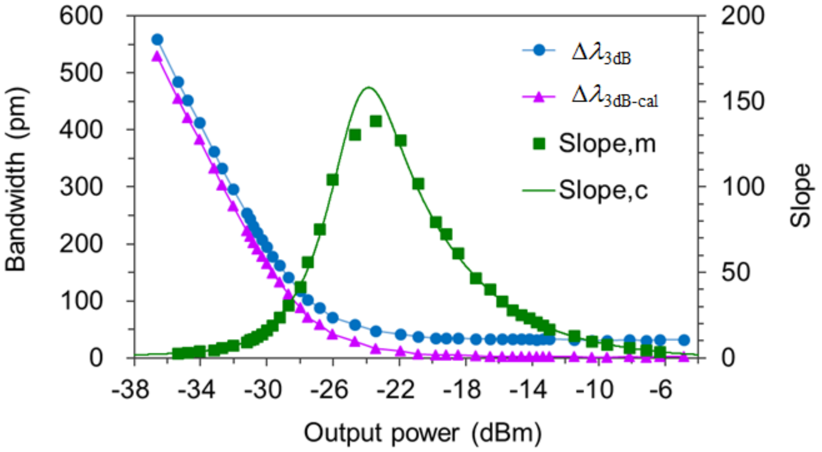

Fig. 5.7 Bandwidth characteristics of the light emitted from the ASEFC. Circles and triangles show measured and calibrated bandwidths, respectively. Measured and calculated slopes are also shown. (Copyright(C) 2023 IEICE, [54] Fig. 7).

The loss of $\mathrm{VOA}_{\mathrm{DUT}}$ was measured in the remote sensing configuration shown in Fig. 5.1(a) by using the ASEFC characteristics that were discussed earlier in this section. The ASEFC was operating in its operational state D at all times. The output power of the ASELS $P_{\mathrm{out\text{-}tot}}$ was 16.7 dBm (47.1 mW), and P_{in} was −5.2 dBm, so that the dynamic range of the sensing system ($\Delta P_{\mathrm{RS}}=P_{\mathrm{out\text{-}tot}}-P_{\mathrm{in}}$) is ~21.9 dB. On the other hand, the total loss of the pair of 50-km SMFs ($\mathrm{SMF}_{\mathrm{up}}$ and $\mathrm{SMF}_{\mathrm{down}}$), 100 km in total, $\mathrm{VOA}_{\mathrm{DUT}}$, and $\mathrm{VOA}_{\mathrm{in}}$ were ~19.0, ~1.0, and ~1.8 dB, respectively. Therefore, the total loss is ~21.9 dB and valances with the dynamic range, equal to ΔP_{RS}. Note that P_{in} was larger than ~6.5 dBm in the case of the ASEFC-P so that the length of each of the paired SMFs was limited to 20 km [28]. $L(d)$, and $L(d)$ is denoted as the loss at a micrometer distance (d) when d equals 0.0 mm is denoted as $L_0 \equiv L(d=0.0\ \mathrm{mm})$. Moreover, the loss difference ($\Delta L_{\mathrm{PM,FC}}(d)$) is defined as

$\Delta L_{\mathrm{a}}(d) \equiv L(d) - L_0$, where a=PM or FC, $\Delta L_{\mathrm{PM}}(d)$ is the difference when the conventional

power meter technique was used with $\mathrm{PD}_{\mathrm{in}}$, and $\Delta L_{\mathrm{FC}}(d)$ is the difference calculated using Eq. (5.1) when our proposed ASEFC was used technique with $\mathrm{PD}_{\mathrm{out}}$. The difference measured in use of the ASEFC technique is denoted as $\Delta L_{\mathrm{FC\text{-}m}}(d)$.

---

[3] This dissertation is based on “Amplified-spontaneous-emission feedback circuit with wide operating bandwidth and dynamic range” [54], by the same author, which appeared in the Proceedings of “IEICE Electronics Express”, Copyright(C) 2023 IEICE.

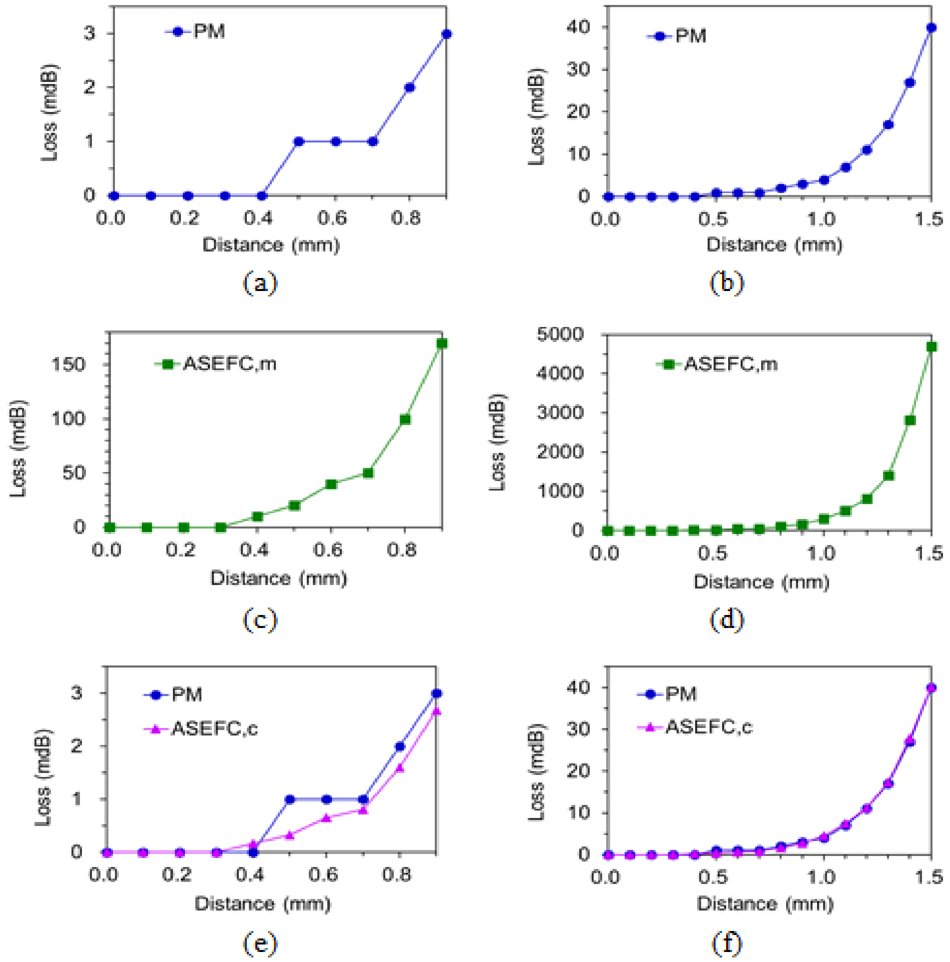

Fig. 5.8 Measured losses of the VOA_{DUT} as a function of the micrometer position in the cases of the conventional technique ((a) and (b)), and of the ASEFC technique ((c) and (d)). Calculated losses for the ASEFC technique are shown in (e) and (f) together with the measured losses for the conventional technique. The regions of the micrometer position for the plots are 0-0.9 mm for (a), (c), and (e), and 0-1.5 mm for (b), (d), and (f). (Copyright(C) 2023 IEICE, [54] Fig. 8).

Figs. 5.8(a) and (b) show the loss difference of conventional technique $\Delta L_{PM}(d)$, Figs. 5.8(c) and (d) show the loss difference of ASEFC technique $\Delta L_{FC\text{-}m}(d)$, and Figs. 5.8(e) and (f) show $\Delta L_{FC}(d)$ together with $\Delta L_{PM}(d)$, as a function of d. Since the light launched into PD_{in} is the ASE from the ASELS, the inaccuracies caused by the interference and polarization effects are thought to be negligible, the minimum display resolution of the digital PM of 0.001 dB was used for $\Delta L_{PM}(d)$. The light launched into PD_{out} was the output light emitted from the ASEFC, so some inaccuracies (0.01 dB estimated) resulting from the interference and polarization effects were expected. On the other hand, the display resolution of 0.01 dB was used for $\Delta L_{FC\text{-}m}(d)$.

[3] This dissertation is based on “Amplified-spontaneous-emission feedback circuit with wide operating bandwidth and dynamic range” [54], by the same author, which appeared in the Proceedings of “IEICE Electronics Express”, Copyright(C) 2023 IEICE.

As shown in Figs. 5.8(a) and (c), it was confirmed that the measurement step was limited to 1 mdB (0.001 dB) and 10 mdB (0.01 dB) for $\Delta L_{\mathrm{PM}}(d)$ and $\Delta L_{\mathrm{FC\text{-}m}}(d)$, respectively, as shown in Figs. 5.8(a) and (c), respectively. From Fig. 5.8(b), the maximum loss variation ($\Delta L_{\max}$), $\Delta L_{\mathrm{PM}}(d)$ at $d = 1.5$ mm, was approximately 40 mdB. P_{in} was selected at $d = 0.0$ mm to be −27.17 dBm using $\mathrm{VOA}_{\mathrm{in}}$ such that $S > 60$ for $\Delta L_{\max}$ of approximately 40 mdB. In reality, S was 61.1 at $d = 0.0$ mm, 65.9 at $d = 0.9$ mm, and 137 at $d = 1.5$ mm (Figs. 4 and 7). Therefore, S values were larger than 61, and OPRs were less than 0.17 mdB (10/61 mdB). Moreover, $\Delta\lambda_{\mathrm{3dB\text{-}cal}}$ was approximately 65 pm at $d = 0.0$ mm (Fig. 5.7) where the corresponding frequency width was 8.2 GHz; As a result, it was determined that the interference and polarization noises were at their lowest at a d value of about 0.0 mm. Figures 5.8(e) and (f) demonstrate that within the experimental accuracy levels in the measurement regions, $\Delta L_{\mathrm{FC}}(d)$ coincided with $\Delta L_{\mathrm{PM}}(d)$).

---

[3] This dissertation is based on “Amplified-spontaneous-emission feedback circuit with wide operating bandwidth and dynamic range” [54], by the same author, which appeared in the Proceedings of “IEICE Electronics Express”, Copyright(C) 2023 IEICE.

5.4 Conclusion of the study

This study presents an ASEFC that uses light with signal wavelengths for the EDF in the C-band as input light for the first time. The operating bandwidth and dynamic range characteristics of ASEFC were experimentally clarified. The ASEFC effectively operated in the 1530-1560 nm wavelength range, with calculated S_{max} values exceeding 100. In addition, to perform remote fiber-optic loss-variation sensing, a pair of 50 km SMFs and $\mathrm{VOA_{DUT}}$ were used in conjunction with the ASEFC and ASELS, following the enhancement of their operating point. The P_{in} value of the ASEFC was around -5.2 dBm, which led to a high dynamic range of approximately 21.9 dB (calculated by ΔP_{RS} ($=P_{\mathrm{out\text{-}tot}} - P_{\mathrm{in}}$)) in the measurement. In addition, it was observed that the improvement factors (S) were greater than 61, and the optical power resolutions (OPRs) were less than 0.17 mdB when using a 10 mdB display resolution on the optical power meter, which was set after the ASEFC in the remote sensing measurement.

---

[3] This dissertation is based on “Amplified-spontaneous-emission feedback circuit with wide operating bandwidth and dynamic range” [54], by the same author, which appeared in the Proceedings of “IEICE Electronics Express”, Copyright(C) 2023 IEICE.

6. Summary

One of the crucial settings in a fiber-optic power meter used in optical communication and measurement systems is optical power resolution (OPR). A novel fiber-optic sensing technique, named the amplified-spontaneous-emission feedback circuit (ASEFC) technique, is proposed in the first study. The technique is implemented in front of a typical optical power meter. Due to operating close to the lasing threshold region, the technique significantly improves OPR. The improvement factor of OPRs was demonstrated by measuring the loss of an optical component using the ASEFC technique. A straightforward analytical function was proposed to describe the relationship between the measurement system's input and output power. The sensitivity or improvement factor of the proposed technique was greater than 67, the OPRs were less than 0.14 mdB initially, and the display resolution of the power meter was set at 10 mdB, where mdB stands for milli dB (10^{-3} dB)

The implementation of a temperature-controlled ASEFC is then proposed as a high-resolution and stable optical power measurement technique in the subsequent study. In order to demonstrate the OPR and stability properties of the temperature-controlled ASEFC technique, two distinct light sources, such as a Fabry-Perot laser and a fiber Bragg grating laser, were employed. The measurement time for determining temporal variations in optical power significantly increased from about five minutes to one hour. An updated fifth-order polynomial function was used in the calculation to represent the input-output relationship with improved accuracy and repeatability. The improvement factors were higher than 97, and the OPRs were greater than 0.10 mdB when the temporal power fluctuation uncertainty of an optical power meter was assumed to equal 10 mdB.

The final study proposed a temperature-controlled ASEFC technique that used the signal wavelength of an EDF as the input light of the measurement system for the first time. Experimental results demonstrated the operating wavelength and dynamic characteristics of the ASEFC. The ASEFC operated at a low input power level of approximately -5.2 dBm. The maximum sensitivity is approximately 100, while operating in the wavelength range of 1530-1560 nm. A small loss variation of a variable optical attenuator was measured by employing the temperature-controlled ASEFC technique with a remote distance of 50 km. The OPRs achieved less than 0.17 mdB and an improvement factor of 61.

7. Future issues

- During the optical loss variation measurement using the ASEFC scheme, it was observed that the output power from the ASEFC fluctuated over time. The forthcoming issue to be addressed is thoroughly examining and optimizing of the time fluctuation mechanism in the ASEFC-based measurement system.
- The proposed ASEFC-based fiber-optic measurement scheme was implemented for a single-mode fiber system in this study. The upcoming task involves implementing the proposed ASEFC-based measurement scheme in multi-mode and multi-core fiber systems.
- The proposed ASEFC scheme operated in the C-band. Building an ASEFC that operates in the L-band within a wavelength range of 1570-1610 nm is possible. Besides the variations in gain block structure and pumping efficiency, C-band and L-band ASEFCs operate using the exact mechanisms. The future challenge will be to extend the operating signal wavelength range of ASEFC-based measurement from C-band to C plus L-band.

8. References

1. A. D. Kersey, “A review of recent developments in fiber optic sensor technology,” Optical Fiber Technol. 2 (1996) 291 (DOI: 10.1006/ofte.1996.0036).
2. A. C. Garcia and J. E. A. Cuenca: in Handbook of Optical Fibre Sensing Technology (John Wiley & Sons, Inc., New Jersey, 2002) ed. J. M. Lopez-Higuera 209.
3. B. Culshaw and A. Kersey: “Fiber-optic sensing: a historical perspective,” J. Lightw. Technol. 26 (2008) 1064 (DOI: 10.1109/JLT.0082.921915).
4. K. Nakazawa, et al., “Technologies for checking outside optical distribution equipment,” NTT Technical Review 7 (2009) 1 (https://www.ntt-review.jp/archive/ntttechnical.php?contents=ntr200911le2.html).
5. B. E. A. Saleh and M. C. Teich, Chap. 19, “Photodetectors” in Fundamentals of Photonics, 3rd ed., B. E. A. Saleh and M. C. Teich, pp. 871-938, John Wiley & Sons, Inc., New Jersey., 2019. ISBN-13:978-1119506874
6. S. Donati: Photodetectors−Devices, Circuits and Applications− (John Wiley & Sons, Inc., New Jersey, 2021) 2nd ed. 103-173.
7. https://www.keysight.com/jp/ja/assets/7018-01006/data-sheets/5988-1569.pdf.
8. https://www.graytechnos.com/60017987/wp-content/uploads/2022/12/manual_211B_212B_213B_20221219.pdf.
9. https://www.hamamatsu.com/content/dam/hamamatsu-photonics/sites/documents/99_SALES_LIBRARY/ssd/g8370-81_etc_kird1064e.pdf.
10. X. G. Huang, et al., “A quasi-distributed fiber-optic temperature sensor with a resolution of 0.07 ℃ based on Fresnel reflection,” J. Lightw. Technol. 27 (2009) 2583 (DOI: 10.1109/JLT.2009.2012411).
11. J.-R. Zhao, et al., “High-resolution and temperature-insensitive fiber optic refractive index sensor based on Fresnel reflection modulated by Fabry–Perot interference,” J. Lightw. Technol. 28 (2010) 2799 (DOI: 10.1109/JLT.2010.2065215).
12. Z. Yin, et al., “Fiber ring laser sensor for temperature measurement,” J. Lightw. Technol. 28 (2010) 3403 (DOI: 10.1109/JLT.2010.2086046).
13. G. Liu, et al., “High-resolution and fast-response fiber-optic temperature sensor using silicon Fabry-Pérot cavity,” Opt. Express 23 (2015) 7237 (DOI: 10.1364/OE.23.007237).

14. S. Diaz: "Stable dual-wavelength erbium fiber ring laser with optical feedback for remote sensing," J. Lightw. Technol. 34 (2016) 4591 (DOI: 10.1109/JLT.2016.2541866).

15. Y. Mizuno, et al., "Pilot demonstration of refractive index sensing using polymer optical fiber crushed with slotted screwdriver," IEICE Electron. Express 14 (2017) 20170962 (DOI: 10.1587/elex.14.20170962).

16. J. Shi, et al., "High-resolution temperature sensor based on intracavity sensing of fiber ring laser," J. Lightw. Technol. 38 (2020) 2010 (DOI: 10.1109/JLT.2019.2954117).

17. K. Fukushima, et al., "EDF laser displacement sensor based on bending characteristics of polarization-independent double-pass cascaded-chirped long-period fiber grating," IEICE Electron. Express 20 (2023) 20220496 (DOI: 10.1587/elex.19.20220496).

18. H. Masuda and K. Kitamura: "Highly sensitive optical sensing scheme using erbium-doped fiber ring circuit," The 7th Asia-Pacific Optical Sensors Conf. (2018) Wed-6.

19. K. Kitamura and H. Masuda: "Nonlinear characteristics of a fiber ring circuit with a semiconductor optical amplifier for sensing applications," The 23rd OECC (2018) 3C1-3 (DOI: 10.1109/OECC.2018.8730129).

20. H. Masuda, et al., "Optically amplified feedback circuit with high improvements in optical power resolution," The 24th OECC (2019) MC2-5 (DOI: 10.23919/PS.2019.8817895).

21. H. Masuda and B. Biswas: "Highly sensitive and stable temperature sensing method using amplified-spontaneous-emission feedback circuit," 26th Microoptics Conf. (2021) MC2-5 (DOI: 10.23919/MOC52031.2021.9598083).

22. B. Biswas, et al., "High-resolution and stable optical power measurement using a temperature controlled amplified-spontaneous-emission feedback circuit," IEICE Comm. Express 12 (2023) 230 (DOI: 10.1587/comex.2023XBL0014).

23. H. Masuda and K. Kitamura: Japan Patent 6660977 (2020).

24. A. E. Siegman, Chap. 13, "Oscillation Dynamics and Oscillation Threshold" in Lasers, pp. 491-557, University Science Books, CA, USA, 1986. ISBN-13:978-0935702118

25. K. Kikuchi, et al., "Lineshape measurement of semiconductor laser below threshold," J. Quantum Elecrtron. 24 (1988) 1814 (DOI: 10.1109/3.7119).

26. M. Ohtsu, et al., "Analyses of mode partition and mode hopping in semiconductor lasers," J. Quantum Elecrtron. 25 (1989) 31 (DOI: 10.1109/3.16237).

27. H. Masuda, et al., “Amplified-spontaneous-emission feedback circuit scheme for optical measurement with improved optical power resolutions,” IEICE Comm. Express 11 (2022) 46 (DOI: 10.1587/comex.2021XBL0189).

28. B. Biswas, et al., “High-resolution and stable optical power measurement using a temperature controlled amplified-spontaneous-emission feedback circuit,” IEICE Comm. Express 12 (2023) 230 (DOI: 10.1587/comex.2023XBL0014).

29. N. Tsukiji and J. Yushida, Chap. 6, “Semiconductor Pump Lasers” in Raman Amplification in Fiber Optical Communication Systems, ed. by C. Headley, G.P. Agrawal, pp. 267-302, Academic Press, Floor, Burlington, USA, 2004. ISBN-13: 978-0120445066

30. M. Maiorov, et al., “Spectral and noise characteristics of Fabry-Perot and DFB 14xx nm InGaAsP/InP pump lasers for Raman and Er-doped fiber amplifiers,” Proc. OFC (2003) 400 (DOI: 10.1109/OFC.2003.1248297).

31. J. Wang, et al., “Noise analysis of semiconductor lasers within the coherence collapse regime,” J. Quantum Elecrtron., vol. 26, no. 9, pp. 1064-1078, May. 2008. (DOI: 10.1109/3.73534).

32. H. Masuda, et al., “1.65 μm band fibre Raman amplifier pumped by wavelength-tunable amplified spontaneous emission light source,” Electron. Lett. 34 (1998) 2339 (DOI: 10.1049/el: 19981543).

33. H. Ono, et al., “1.58-μm band gain-flattened erbium-doped fiber amplifiers for WDM transmission systems,” J. Lightw. Technol. 17 (1999) 490 (DOI: 10.1109/50.749390).

34. H. Masuda and Y. Miyamoto: “Low-noise extended L-band phosphorus co-doped silicate EDFA consisting of novel two-stage gain-flattened gain blocks,” Electron. Lett. 44 (2008) 1082 (DOI: 10.1049/el: 20081520).

35. H. Masuda, et al., “Wideband erbium-doped fibre amplifiers with three-stage amplification,” Electron. Lett. 34 (1998) 567 (DOI: 10.1049/el: 19980432).

36. A. Sano, et al., “Ultra-high capacity WDM transmission using spectrally-efficient PDM 16-QAM modulation and C- and extended L-band wideband optical amplification,” J. Lightw. Technol. 29 (2011) 578 (DOI: 10.1109/JLT.2011.2107030).

37. B. Biswas, et al., “Output Wavelength Dependence of the Performance of an Optically Amplified Feedback Circuit,” IEICE Society Conference, B-13-2 (2019).

38. B. Biswas, et al., “Optimization of the Output Wavelength of an Optically Amplified Feedback Circuit for a Multi-wavelength Optical Sensing System,” HISS, 21st, B1-22, pp.332-334(2019), (Domestic Conference with Review).
39. B. Biswas, et al., “Numerical Simulation on Wavelength Characteristics of an Optically Amplified Feedback Circuit for Multi-Wavelength Sensing Applications,”The67thJSAPSpringMeeting, 14p-B409-15(2020).
40. B. Biswas and H. Masuda: “Numerical Simulation on the Performance of an Amplified-Spontaneous- Emission Feedback Circuit in Optical Power Sensing Application,” IEICE General Conference, B-13-10 (2021).
41. B. Biswas and H. Masuda: “Remote Temperature Sensing with an Amplified-Spontaneous-Emission Feedback Circuit,” IEICE Society Conference, B-13-2 (2021).
42. H. Masuda, et al., “Optically-amplified feedback photo-detector with significantly small resolution,” 11a-W935-7 (in Japanese), The 66th JSAP Spring Meeting (2019).
43. MD Syful Islam, et al., “Loop Loss Dependence of the Performance of an Optically Amplified Feedback Circuit,” B-13-3, IEICE Society Conference (2019).
44. MD Syful Islam, et al., “Optimization of the Loop Loss of an Optically Amplified Feedback Circuit for Optical Power Sensing Systems,” A1-22, pp. 69-71, HISS 21st Conference (2019) (Domestic Conference with Review).
45. Md Syful Islam, et al., “Numerical Simulation on the Loop-loss Dependence of the Performance of an Optically Amplified Feedback Circuit,” 14p-B409-11, The 67th JSAP Spring Meeting (2020).
46. H. Masuda, et al., “Optical Loss Measurement Using an Amplified-Spontaneous-Emission Feedback Circuit with High Improvements in Optical Power Resolution,” B-13-7, IEICE Society Conference (2020).
47. H. Masuda, et al., A Novel Optical Power Measurement Scheme Using an Amplified-Spontaneous-Emission Feedback Circuit with High Improvements in Optical Power Resolution,” IEICE Technical Report, OFT-2020-40, pp.17-20 (2020).
48. H. Masuda and B. Biswas: “Highly Sensitive and Stable Temperature Sensing Method Using Amplified Spontaneous-Emission Feedback Circuit,” 26th Micro-optics Conference (2021) (International Conference with Review). (DOI: 10.23919/MOC52031.2021.9598083).

49. Hiroji Masuda and B. Biswas: “Theoretical Investigation on the Performance of an Amplified-Spontaneous-Emission Feedback Circuit in Optical Power Measurement,” OFT-2020-64, pp.38-43, IEICE Technical Report (2021).

50. Hiroji Masuda, et al., “Fiber-Optic Temperature Sensing Method Using an Amplified-Spontaneous-Emission Feedback Circuit,” B-13-1, IEICE Society Conference (2021).

51. Kunihiro Tanaka, et al., “Fiber-Optic Temperature Sensing with Amplified Spontaneous Emission from Erbium-Doped Fiber,” The 72nd Annual Meeting of the Chugoku Branch of the Electrical and Information Society (2021).

52. Hiroji Masuda, et al., “Fiber-Optic Temperature Sensing with High Resolution and Stability by Detecting Amplified Spontaneous Emission,” OECC (2022). (DOI: 10.23919/OECC/PSC53152.2022.9850201).

53. Hiroji Masuda, et al., “Design and Performance of an Amplified Spontaneous-Emission Feedback Circuit for Fiber-Optic Temperature Sensing,” IEICE Technical Reports, OFT2022-16, Vol.122, No.162, pp. 50-55 (2022).

54. Biswajit Biswas, et al., “Amplified-spontaneous-emission feedback circuit with wide operating bandwidth and dynamic range,” ELEX Electronics Express. [Accepted, July, 2023] (DOI:10.1587/elex.20.20230229)

55. H. Masuda, et al., "Highly sensitive Raman gain coefficient measurement by detecting spontaneous Raman scattering power for distributed Raman amplification systems", IEICE Commun. Exp, vol. 6, pp. 661-666, Oct. 2017. (DOI:10.1587/comex.2017XBL0121).

56. H. Masuda, et al., "Distributed optical amplification technologies for multicore fiber transmission", 2016 IEEE Photonics Society Summer Topical Meeting on SDM for Optical Comm, pp. 76-77, Jul. 2016. (DOI: 10.1109/PHOSST.2016.7548735).

57. W. Lin, et al., “Review on Development and Applications of Fiber-Optic Sensors,” IEEE Symposium on Photonics and Optoelectronics (2012). (DOI: 10.1109/SOPO.2012.6270996).

58. Z. Yin, et al., “Fiber ring sensor for temperature measurement,” J. Lightw. Technol., vol. 28, no. 23, pp. 3403-3408, (2010). (DOI: 10.1109/JLT.2010.2086046).

59. K. W. Quoi, et al., “Rare-earth doped fibers for temperature sensing,” J. Lightw. Technol., vol. 10, no. 6, pp. 847-852, (1992). (DOI: 10.1109/50.143086).

60.K. Kyuma, et al., “Rare-earth doped fibers for temperature sensing,” J. Quantum Electronics, vol. QE-18, no. 4, pp. 676-679, (1982).

61. W. Eichoff, et al., “Temperature sensing by mode-mode interference in birefringent optical fibers,” Optics Letters, vol. 6, no. 4, pp. 204-206, (1981). (DOI:10.1364/OL.6.000204).

62. K. W. Quoi, et al., “Laser temperature sensor based on a fiber Bragg grating,” IEEE Photon. Technol. Lett., vol. 27, no. 11, pp. 1141-1144, (2015). (DOI: 10.1109/LPT.2015.2406572).

63. J. Mandal, et al., “Bragg grating-based fiber-optic laser probe for temperature sensing,” IEEE Photon. Technol. Lett., vol. 16, no. 1, pp. 218-220, (2004). (DOI: 10.1109/LPT.2003.820099).

64. I. Hernandez-Romano, et al., “Highly sensitive temperature sensor based on a polymer-coated microfiber interferometer,” IEEE Photon. Technol. Lett., vol. 27, no. 24, pp. 2591-2594, (2015). (DOI: 10.1109/LPT.2015.2478790).

65. Y. Liu, et al., “Microcapillary-based high-sensitivity and wavelength-tunable optical temperature sensor,” IEEE Photon. Technol. Lett., vol. 27, no. 4, pp. 447-450, (2015). (DOI: 10.1109/LPT.2014.2377195).

66. N. J. C. Libatique, et al., “A broadly tunable wavelength-selectable WDM source using a fiber Sagnac loop filter,” IEEE Photon. Technol. Lett., vol. 13, no. 12, pp. 1283-1285, (2001). (DOI: 10.1109/68.969882).

67. M. Fernandez-Vallejo, et al., “Comparison of the stability of ring resonator structures for multiwavelength fiber lasers using Raman or Er-doped fiber amplification,” IEEE J. Quantum Electronics., vol. 45, no. 12, pp. 1551-1557, (2009). (DOI: 10.1109/JQE.2009.2028618).

68. E. Maurice, et al., “Erbium-doped silica fibers for intrinsic fiber-optic temperature sensors,” Applied Optics, vol. 34, no. 34, pp. 8019-8025, (1995). (DOI: 10.1364/AO.34.008019).

69. E. Maurice, et al., “1.2-μm transitions in erbium-doped fibers: the possibility of quasi-distributed temperature sensors,” Applied Optics, vol. 34, no. 21, pp. 4196-4199, (1995). (DOI: 10.1364/AO.34.004196).

70. E. Maurice, et al., “Self-referenced point temperature sensor based on a fluorescence intensity ratio in Yb^{3+}-doped silica fiber,” Applied Optics, vol. 36, no. 31, pp. 8264-8269, (1997). (DOI: 10.1364/AO.36.008264).

71. E. Maurice, et al., “High dynamic range temperature point sensor using green fluorescence intensity ratio in erbium-doped silica fiber,” IEEE Photon. Technol. Lett., vol. 13, no. 7, pp. 1349-1353, (1995). (DOI: 10.1109/50.400677).

72. J. Peng, et al., “High temperature sensing characteristics of erbium-doped fiber using fluorescence intensity ratio technology,” Proc. Of SPIE-OSA-IEEE, vol. 7630, pp. 76300B-1-76300B-6, (2009).

73. C. Layne, et al., “ Nonradiative relaxation of rare-earth ions in silicate laser glass” , IEEE Journal of Quantum Electronics, Vol. 11, No. 9, pp. 788-799, (1975) (DOI: 10.1109/JQE.1975.1068921).

74. N. Kagi , et al., “ Temperature dependence of the gain in erbium-doped fibers” , IEEE Journal of Lightwave Technology, Vol. 9, No. 2, pp. 261-265, (1991) (DOI: 10.1109/50.658849.

75. Michael J. Yadlowsky, et al., "Pump Wavelength-Dependent Spectral-Hole Burning in EDFA's," J. Lightwave Technol. 17, 1643- (1999)

76. Z. Yin et al., "Fiber Ring Laser Sensor for Temperature Measurement," in Journal of Lightwave Technology, vol. 28, no. 23, pp. 3403-3408, Dec.1, 2010, (DOI: 10.1109/JLT.2010.2086046).

77. Jia Shi, et al., "High-Resolution Temperature Sensor Based on Intracavity Sensing of Fiber Ring Laser," J. Lightwave Technol. 38, 2010-2014 (2020).

78. W. L. BARNES, et al., "Absorption-emission cross-section ratio for Er3+ doped fibers" in IEEE Journal of Quantum Electronics, vol. 27, no. 4, pp. 1004-1010, (1991).

79. M. Yamada, et al., "Temperature Insensitive Er3+-doped Optical Fiber Amplifiers," in Optical Amplifiers and Their Applications, Technical Digest Series (Optica Publishing Group, 1990), paper PDP7.

80. R. Feced, et al., "Acousto-optic attenuation filters based on tapered optical fibers," in IEEE Journal of Selected Topics in Quantum Electronics, vol. 5, no. 5, pp. 1278-1288, Sept.-Oct. 1999, (DOI: 10.1109/2944.806753).

81. E. Desurvire, et al., "Analysis of erbium-doped fiber amplifiers pumped in the /sup 4/I/sub 15/2/-/sup 4/I/sub 13/2/ band," in IEEE Photonics Technology Letters, vol. 1, no. 10, pp. 293-296, Oct. 1989, (DOI: 10.1109/68.43353).

82. M. Yamada, et al., " Noise Characteristics of Er^{3+} -Doped Fiber Amplifiers Pumped by 0.98 and 1.48µm Laser Diodes," in IEEE Photonics Technology Letters, vol. 2, no. 3, pp. 205-207 (1990).

83. M. Shimizu, et al., "Concentration effect on optical amplification characteristics of Er-doped silica single-mode fibers," in IEEE Photonics Technology Letters, vol. 2, no. 1, pp. 43-45, Jan. 1990, (DOI: 10.1109/68.47037).

84. N. Kagi, et al., "Efficient optical amplifier using a low-concentration erbium-doped fiber," in IEEE Photonics Technology Letters, vol. 2, no. 8, pp. 559-561, Aug. 1990, (DOI: 10.1109/68.58048).

85. T. Pfeiffer, et al., "Analytical gain equation for erbium-doped fiber amplifiers including mode field profiles and dopant distribution," in IEEE Photonics Technology Letters, vol. 4, no. 5, pp. 449-451, May 1992, (DOI: 10.1109/68.136482).

86. S. L. Hansen, et al., "Gain limit in erbium-doped fiber amplifiers due to internal Rayleigh backscattering," in IEEE Photonics Technology Letters, vol. 4, no. 6, pp. 559-561, June 1992, (DOI: 10.1109/68.141967).

87. T. Pfeiffer, et al., "Output power characteristics of erbium-doped fiber ring lasers," in IEEE Photonics Technology Letters, vol. 4, no. 8, pp. 847-849, Aug. 1992, (DOI: 10.1109/68.149883).

88. G. A. Ball, et al., "Single- and multipoint fiber-laser sensors," in IEEE Photonics Technology Letters, vol. 5, no. 2, pp. 267-270, Feb. 1993, (DOI: 10.1109/68.196026).

89. G. A. Ball, et al., "Modeling of short, single-frequency, fiber lasers in high-gain fiber," in IEEE Photonics Technology Letters, vol. 5, no. 6, pp. 649-651, June 1993, (DOI: 10.1109/68.2196989.

90. M. Yamada et al., "Fluoride-based erbium-doped fiber amplifier with inherently flat gain spectrum," in IEEE Photonics Technology Letters, vol. 8, no. 7, pp. 882-884, July 1996, (DOI: 10.1109/68.502258).

91. P. F. Wysocki, et al., "Broad-band erbium-doped fiber amplifier flattened beyond 40 nm using long-period grating filter," in IEEE Photonics Technology Letters, vol. 9, no. 10, pp. 1343-1345, Oct. 1997, (DOI: 10.1109/68.623257).

92. Shien-Kuei Liaw, et al., "Dynamic power-equalized EDFA module based on strain tunable fiber Bragg gratings," in IEEE Photonics Technology Letters, vol. 11, no. 7, pp. 797-799, July 1999, (DOI: 10.1109/68.769711).

93. Shenping Li, et al., "Gain flattening of an erbium-doped fiber amplifier using a high-birefringence fiber loop mirror," in IEEE Photonics Technology Letters, vol. 13, no. 9, pp. 942-944, Sept. 2001, (DOI: 10.1109/68.942654).

94. J. Shi, et al., "Temperature Self-Compensation High-Resolution Refractive Index Sensor Based on Fiber Ring Laser," in IEEE Photonics Technology Letters, vol. 29, no. 20, pp. 1743-1746, 15 Oct.15, 2017, (DOI: 10.1109/LPT.2017.2751753).

95. C. -L. Lee, et al., "Highly Sensitive Air-Gap Fiber Fabry–Pérot Interferometers Based on Polymer-Filled Hollow Core Fibers," in IEEE Photonics Technology Letters, vol. 24, no. 2, pp. 149-151, Jan.15, 2012, (DOI: 10.1109/LPT.2011.2174632).

96. L. Liang, et al., "Refractive Index and Temperature Sensor Based on Fiber Ring Laser With STCS Fiber Structure," in IEEE Photonics Technology Letters, vol. 26, no. 21, pp. 2201-2204, 1 Nov.1, 2014, (DOI: 10.1109/LPT.2014.2350151).

97. J. Shi et al., "Temperature Sensor Based on Fiber Ring Laser With Sagnac Loop," in IEEE Photonics Technology Letters, vol. 28, no. 7, pp. 794-797, 1 April1, 2016, (DOI: 10.1109/LPT.2015.2514105).

98. C. Spiegelberg, et al., "Low-noise narrow-linewidth fiber laser at 1550 nm (June 2003)," in Journal of Lightwave Technology, vol. 22, no. 1, pp. 57-62, Jan. 2004, (DOI: 10.1109/JLT.2003.822208).

99. F. Farahi, et al., "Simultaneous measurement of temperature and strain: cross-sensitivity considerations," in Journal of Lightwave Technology, vol. 8, no. 2, pp. 138-142, Feb. 1990, (DOI: 10.1109/50.47862).

100. H. Li, et al., "Centimeter Spatial Resolution Distributed Temperature Sensor Based on Polarization-Sensitive Optical Frequency Domain Reflectometry," in Journal of Lightwave Technology, vol. 39, no. 8, pp. 2594-2602, 15 April15, 2021, (DOI: 10.1109/JLT.2021.3052036).

101. T. Kurashima, et al., "Thermal effects of Brillouin gain spectra in single-mode fibers," in IEEE Photonics Technology Letters, vol. 2, no. 10, pp. 718-720, Oct. 1990, (DOI: 10.1109/68.60770).

102. G. J. Cowle et al., "Multiple wavelength generation with Brillouin/erbium fiber lasers," in IEEE Photonics Technology Letters, vol. 8, no. 11, pp. 1465-1467, Nov. 1996, (DOI: 10.1109/68.541551).

103. Y. Zhang, et al., "Super-High Sensitivity of Fiber Temperature Sensor Based on Leaky-Mode Bent SMS Structure," in IEEE Photonics Technology Letters, vol. 25, no. 6, pp. 560-563, March15, 2013, (DOI: 10.1109/LPT.2013.2245644).

104. Y. Zhao, et al., "Temperature Sensing Characteristics Based on Up-Taper and Single Mode–Multimode Fiber Structure," in IEEE Photonics Technology Letters, vol. 28, no. 22, pp. 2557-2560, 15 Nov.15, 2016, (DOI: 10.1109/LPT.2016.2605675).

105. H. Masuda, et al., "Modeling the gain degradation of high concentration erbium-doped fiber amplifiers by introducing inhomogeneous cooperative up-conversion," in Journal of Lightwave Technology, vol. 10, no. 12, pp. 1789-1799, Dec. 1992, (DOI: 10.1109/50.202830).

106. E. Desurvire, Erbium-Doped Fiber Amplifiers, John Wiley & Sons, Inc., Chap. 1 (1994).